The giant Mauritanian cold-water coral mound province: Oxygen control on coral mound formation

Claudia Wienberg, Jürgen Titschack, André Freiwald, Norbert Frank, Tomas Lundälv, Marco Taviani, Lydia Beuck, Andrea Schröder-Ritzrau, Thomas Krengel, Dierk Hebbeln

Quaternary Science Reviews 185 (2018) 135–152

Contents lists available at ScienceDirect

Quaternary Science Reviews

journal homepage: www.elsevier.com/locate/quascirev

The giant Mauritanian cold-water coral mound province: Oxygen control on coral mound formation

Claudia Wienberg [a, *], Jürgen Titschack [a, b], André Freiwald [b], Norbert Frank [c, d], Tomas Lundälv [e], Marco Taviani [f, g, h], Lydia Beuck [b], Andrea Schröder-Ritzrau [c], Thomas Krengel [c], Dierk Hebbeln [a]

[a] Center for Marine Environmental Sciences (MARUM), Bremen University, Leobener Strasse 2, 28359 Bremen, Germany
[b] Senckenberg am Meer (SAM), Marine Research Department, Südstrand 40, 26382 Wilhelmshaven, Germany
[c] Institute of Environmental Physics (IUP), Heidelberg University, Im Neuenheimer Feld 229, 69120 Heidelberg, Germany
[d] Laboratoire des Sciences du Climat et de l'Environnement (LSCE), Bât.12, Avenue de la Terrasse, F-91198 Gif-sur-Yvette, France
[e] Swedish Institute for the Marine Environment, University of Gothenburg, 45296 Strömstad, Sweden
[f] Istituto di Scienze Marine (ISMAR-CNR), Via Gobetti 101, 40129 Bologna, Italy
[g] Biology Department, Woods Hole Oceanographic Institution, 266 Woods Hole Road, Woods Hole, MA 02543, USA
[h] Stazione Zoologica Anton Dohrn, Villa Comunale, 80121 Naples, Italy

ARTICLE INFO

Article history:
Received 3 July 2017
Received in revised form
29 January 2018
Accepted 11 February 2018
Available online 20 February 2018

Keywords:
Lophelia pertusa
Coral mound
Submarine canyon
Uranium-series dating
Mound aggradation rate
Last glacial
Dissolved oxygen concentration
South Atlantic Central Water
Mauritanian margin

ABSTRACT

The largest coherent cold-water coral (CWC) mound province in the Atlantic Ocean exists along the Mauritanian margin, where up to 100 m high mounds extend over a distance of ~400 km, arranged in two slope-parallel chains in 400–550 m water depth. Additionally, CWCs are present in the numerous submarine canyons with isolated coral mounds being developed on some canyon flanks. Seventy-seven Uranium-series coral ages were assessed to elucidate the timing of CWC colonisation and coral mound development along the Mauritanian margin for the last ~120,000 years. Our results show that CWCs were present on the mounds during the Last Interglacial, though in low numbers corresponding to coral mound aggradation rates of 16 cm kyr^{-1}. Most prolific periods for CWC growth are identified for the last glacial and deglaciation, resulting in enhanced mound aggradation (>1000 cm kyr^{-1}), before mound formation stagnated along the entire margin with the onset of the Holocene. Until today, the Mauritanian mounds are in a dormant state with only scarce CWC growth. In the canyons, live CWCs are abundant since the Late Holocene at least. Thus, the canyons may serve as a refuge to CWCs potentially enabling the observed modest re-colonisation pulse on the mounds along the open slope. The timing and rate of the pre-Holocene coral mound aggradation, and the cessation of mound formation varied between the individual mounds, which was likely the consequence of vertical/lateral changes in water mass structure that placed the mounds near or out of oxygen-depleted waters, respectively.

1. Introduction

Cold-water coral (CWC) mounds formed by framework-building scleractinian CWCs (mainly *Lophelia pertusa*) are widely distributed along the continental margins of the Atlantic Ocean (Hebbeln and Samankassou, 2015; Roberts et al., 2009). They occur from shelf environments down to the upper and middle slopes (<1000 m water depth) and are mostly arranged in large provinces that comprise hundreds of individual mounds and cover extensive areas of several tens of square kilometres (e.g., Fosså et al., 2005; Glogowski et al., 2015; Grasmueck et al., 2006; Hebbeln et al., 2014; Paull et al., 2010; Vandorpe et al., 2017; Wheeler et al., 2007). Coral mounds are the result of a complex interplay between CWC growth and sediment input. In particular, the capability of the coral framework to baffle current-transported sediments plays a crucial role as the entrapped sediments stabilize the biogenic construction, and hence, favour mound aggradation (Huvenne et al., 2009; Thierens et al., 2013; Titschack et al., 2015, 2016). Consequently, coral mounds can develop into impressive seabed structures up to 300 m high and several kilometres in

* Corresponding author.
E-mail address: cwberg@marum.de (C. Wienberg).

https://doi.org/10.1016/j.quascirev.2018.02.012

diameter that are deposited over many thousands to even millions of years (Kano et al., 2007; Roberts et al., 2006). Hence, coral mounds offer important records to reconstruct (i) the population history of CWCs with recurring periods of CWC growth and decline, and (ii) the temporal variability in vertical mound aggradation, alternating between active and dormant mound stages (Wienberg and Titschack, 2017). Moreover, the widespread occurrence and large dimension of coral mounds highlight their crucial role in continental margin architecture (De Mol et al., 2009; Hebbeln et al., 2016) and their relevance as important carbonate factories forming significant sinks for inorganic carbon (Lindberg and Mienert, 2005; Titschack et al., 2016). Due to their age and enhanced aggradation, they also provide unique archives of environmental and climate change, even preserving stratigraphic records lacking in the neighbouring sedimentary succession where simultaneously erosion or non-deposition prevailed (e.g., Frank et al., 2011; Hebbeln et al., 2016; Thierens et al., 2013; Titschack et al., 2009).

Much progress has been made in recent years to decipher the temporal development of Atlantic coral mounds across major climate changes, such as those induced by glacial-interglacial variability (Frank et al., 2009; Kano et al., 2007; López Correa et al., 2012; Raddatz et al., 2014; van der Land et al., 2014; Wienberg et al., 2010). For the Northeast Atlantic, it was demonstrated that areas offering optimal conditions for sustained coral mound formation have shifted latitudinally in pace with major climate changes (Frank et al., 2011). The opposing settings are characterized by coral mound provinces along the NW European margin, whose most recent formation period occurred during the Holocene associated with very high vertical mound aggradation rates (ARs) of 200–1500 cm kyr^{-1} (Dorschel et al., 2005; Douarin et al., 2013; López Correa et al., 2012; Titschack et al., 2015; Victorero et al., 2016). In contrast, mound formation was active along the NW African margin during the last glacial (and former glacial periods), ceased with the onset of the Holocene, and remained in a dormant state until today (Eisele et al., 2011; Wienberg et al., 2009, 2010). First studies of coral mound provinces in the Northwest Atlantic revealed a predominantly interglacial mound formation along the US margin (Cape Lookout) and in the southern Gulf of Mexico (Campeche Bank) (Matos et al., 2015, 2017).

Beside the assessment of the temporal development of coral mounds and of any large-scale pattern or basin-wide relation between the different provinces in the Atlantic, the understanding of the environmental and oceanographic factors controlling mound formation today and in the past is of main interest. This knowledge is essential to assess the response of these important deep-sea ecosystems to future ocean circulation changes, increasing water temperatures, and ocean acidification (Guinotte et al., 2006; Orr et al., 2005; Turley et al., 2007). The formation of coral mounds foremost depends on sustained CWC growth, which is in turn controlled by specific environmental boundary conditions. These encompass (i) physical and chemical properties of the surrounding bottom water masses (e.g., temperature, dissolved oxygen concentration (DOC), aragonitic saturation state, pH); (ii) the availability of sufficient food steered by enhanced surface ocean productivity; and (iii) the local hydrodynamic regime providing a constant to periodic delivery of suspended food particles to the sessile suspension-feeding CWCs (e.g., Büscher et al., 2017; Davies et al., 2009; Davies and Guinotte, 2011; Duineveld et al., 2012; Flögel et al., 2014; Mienis et al., 2007; Thresher et al., 2011; White et al., 2005). However, even if environmental conditions are within the constraints for CWC growth, coral mounds do not necessarily develop or turn from a dormant into an active state assuming that environmental controls on mound formation are far more complex and restrictive (Wienberg and Titschack, 2017). Nevertheless, regional studies indicate that mound formation depends on a dynamic bottom current regime (e.g., increased bottom current strength controlling food supply; Dorschel et al., 2005; Eisele et al., 2008; Matos et al., 2015) and enhanced palaeoproductivity (Eisele et al., 2011; Wienberg et al., 2010), while low bottom water oxygenation might present a major stressor (Fink et al., 2012). Overall, the regional environmental conditions stimulating or suppressing coral mound formation are strongly linked to the water column structure and water mass circulation at intermediate water depths (Fink et al., 2015; Henry et al., 2014; Matos et al., 2017). However, although our knowledge on coral mound formation steadily increased with every new coral mound province being discovered, it is still fragmentary.

In this study, the temporal development of the present-day world's largest coherent coral mound province along the Mauritanian margin is described and assessed. The Mauritanian coral mound province consists of up to 100-m-high coral mounds, which are arranged in two slope-parallel chains distributed over ~400 km (Figs. 1 and 2; Ramos et al., 2017). Today, the Mauritanian mounds are in a dormant state, deduced by the current scarcity of living CWCs. However, live CWCs are more frequently described from the numerous submarine canyons in the region (Westphal et al., 2012). The knowledge about the timing of CWC colonisation and coral mound development off Mauritania as well as of any

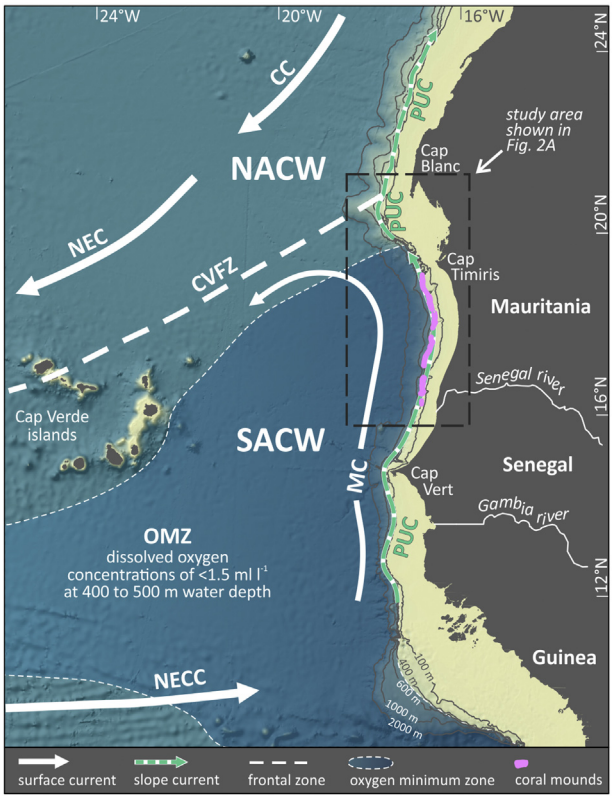

Fig. 1. Map showing the schematic oceanic circulation pattern along the NW African margin (source of bathymetry data: www.gebco.net). Shown are the main surface (white arrow; CC: Canary Current, NEC: North Equatorial Current, MC: Mauritanian Current, NECC: North Equatorial Countercurrent) and slope currents (green dashed arrow; PUC: Poleward Undercurrent), and the position of the Cap Verde frontal zone (CVFZ; bold dashed white line) separating the North and South Atlantic Central Waters (NACW, SACW). The extension of the oxygen minimum zone (OMZ) with DOCs of <1.5 ml l^{-1} at 400–500 m water depth is indicated (blue colour with white dashed edging; modified after Arístegui et al., 2009; Peña→Izquierdo et al., 2012, 2015). The Mauritanian cold-water coral mound province is marked by pink stripes (according to Ramos et al., 2017; for details see Fig. 2). (For interpretation of the references to colour in this figure legend, the reader is referred to the Web version of this article.)

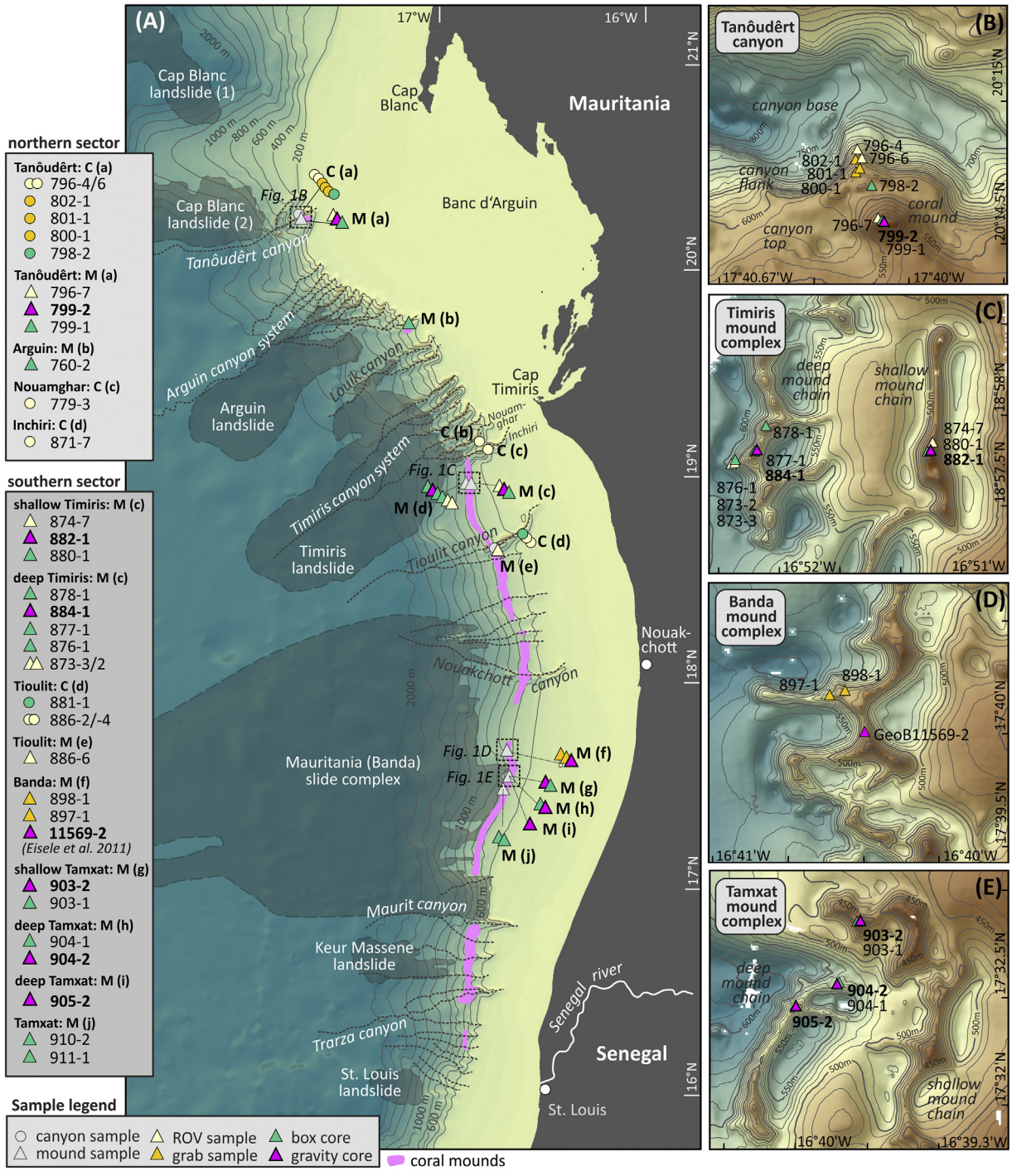

Fig. 2. **(A)** Bathymetric overview map showing the Mauritanian margin (data source: www.gebco.net) with its numerous canyons and gullies (grey dashed sinusoidal lines) and partly giant landslides (transparent patches; extent of landslides according to Jakobi and Hayes, 1982; Henrich et al., 2008; Sanz et al., 2017). In the northern sector, coral mounds are occasionally developed on top of some canyon flanks. The southern sector shows a complex system of coral mounds extending over a distance of ~400 km (pink stripes; according to Colman et al., 2005; Westphal et al., 2012; Ramos et al., 2017). **(B–E)** Detailed maps of **(B)** the Tanôudêrt canyon with a circular 60-m-high coral mound developed at the top of its southern flank, and **(C)** the Timiris mound complex with two mound chains developed, **(D)** the honeycomb-like Banda mound complex, and **(E)** the Tamxat mound complex with two mound chains developed (data source: https://doi.pangaea.de/10.1594/PANGAEA.883754; Wintersteller et al., 2017). Sites from which coral material were collected during R/V Maria S. Merian cruise MSM16-3 are indicated as triangles (samples from coral mounds) and dots (samples from canyons). The respective sample-IDs (GeoB14 xxx-x) are provided in the grey-shaded boxes to the left, including core GeoB11569-2 (Eisele et al., 2011). (For interpretation of the references to colour in this figure legend, the reader is referred to the Web version of this article.)

environmental control on mound formation is still limited (Eisele et al., 2011, 2014). To overcome this limitation, this study provides a comprehensive dataset of Uranium-series ages obtained from coral material that is collected from a ~300-km-long latitudinal transect encompassing several coral mounds but also submarine canyons (Fig. 2). The main aims of this study are (i) to confirm and refine the proposed last glacial CWC proliferation for the entire Mauritanian margin; (ii) to elucidate local and regional coral mound formation patterns by comparing vertical mound ARs from mounds developed at different water depths (upper and lower coral mound chains) along an extended N-S transect; (iii) to conduct a first assessment of environmental controls that steered CWC growth and coral mound formation; and (iv) to examine the CWC colonisation of different habitats, namely submarine canyons and coral mounds, potentially offering differing environmental boundary conditions. The obtained results from the giant Mauritanian coral mound province highlight the spatiotemporal complexity in mound development constrained by a very particular environmental setting. This study elucidates coral mound formation within an oxygen minimum zone (OMZ; Fig. 1; Karstensen et al., 2008) and below one of the most important upwelling, and consequently, most productive areas in the marine realm (Behrenfeld and Falkowski, 1997; Carr and Kearns, 2003).

2. The Mauritanian margin

2.1. Submarine canyons and landslides

The N-S-oriented Mauritanian continental margin can be subdivided into two sectors (Fig. 2A). The northern part stretches from Cap Blanc to Cap Timiris and is bordered to the east by the Banc d'Arguin, where the Mauritanian shelf has its greatest width with ~150 km (e.g., Hanebuth and Lantzsch, 2008). The southern part, extending between Cap Timiris and the Senegalese border, has an arced configuration and is connected to a very narrow shelf ranging in width between 25 and 40 km. The Mauritanian slope is dissected by numerous gullies that merge into partly giant submarine canyon systems with the northern Arguin and Timiris canyon systems extending basinward over several hundreds of kilometres (Fig. 2A; e.g., Antobreh and Krastel, 2006). The canyons connect the shelf area with the deep sea and serve as major conduits for turbidity currents that transport large amounts of sediments from the shelf and the upper slope into the abyss (e.g., Henrich et al., 2010). The Mauritanian canyons are today not connected to any large river system, instead they occur offshore the Sahara desert, from where large quantities of aeolian sediments are transported to and deposited off Mauritania (Harrison et al., 2001). The Senegal river at the southern Mauritanian border (Fig. 2A) is the only presently active drainage system in the area (Roudier et al., 2014). Additionally, several large landslides are reported along the entire Mauritanian margin, which are associated with the canyons (e.g., Jakobi and Hayes, 1982; Sanz et al., 2017; Wien et al., 2007). Most prominent is the Mauritania (Banda) slide complex along the southern sector (Fig. 2A), which represents with a coverage area of ~34.000 km^2 one of the largest slope failures along the NE Atlantic margin (Antobreh and Krastel, 2007; Henrich et al., 2008).

2.2. Cold-water corals and coral mounds

Scleractinian CWCs are common along the entire Mauritanian margin, where they predominantly occur as fossil deposits within the numerous submarine canyons and on the coral mounds (Fig. 3; Colman et al., 2005; Westphal et al., 2012). Live CWCs were observed in rather low numbers on top of the coral mounds, and frequently attached to the canyon walls, partly forming reef-like structures (Westphal et al., 2012). *Lophelia pertusa* is overall the dominant coral species off Mauritania (Fig. 3), while *Madrepora oculata*, *Dendrophyllia cornigera*, *Solenosmilia variabilis* and solitary CWCs such as *Desmophyllum dianthus* and caryophylliid species are just minor constituents to the coral community (Colman et al., 2005; Westphal et al., 2012).

The Mauritanian coral mounds were first described by Colman et al. (2005). Up to 100-m-high mound structures were identified, which are aligned parallel to the coastline in water depths between 400 and 550 m (Colman et al., 2005). Subsequent Spanish and German expeditions (R/V Poseidon cruise P346, R/V Vizconde de Eza cruises MAURIT-0811, -0911, –1011, R/V Maria S. Merian cruise MSM16-3; Ramos et al., 2010; Westphal et al., 2007, 2012) revealed that the coral mounds cover almost the entire margin between Cap Timiris and the Senegalese border (Fig. 2A; Ramos et al., 2017). The Mauritanian coral mounds show a rather uncommon morphological configuration compared to other known coral mound areas in the North Atlantic. They are merged to an almost continuous chain, in places, two sub-parallel mound chains are present following distinct water depth levels (Fig. 2C–E; Colman et al., 2005; Ramos et al., 2017; Westphal et al., 2012). Their appearance is highly variable and varies from elongated and straight to arcuate shapes. Arcuate mounds often coalesce, thereby forming very complex structures (Fig. 2C–E). The Mauritanian coral mounds are bounded to the east and west by moats of 20–50 m depth (Colman et al., 2005; Ramos et al., 2017). Locally, the mound chains are interrupted by canyons and gullies or are buried by sediment slides (Ramos et al., 2017). Coral mounds belonging to the Tamxat mound complex are located just upslope of the headwall scarp of the large Mauritania slide complex (Fig. 2A; see also De Mol et al., 2009). North of Cap Timiris, the coral mound chain seems to vanish and can barely be tracked between the numerous canyons of this northern margin sector (Ramos et al., 2017; Westphal et al., 2012). However, single mounds developed on the flanks of some canyons (e.g., Tanôudêrt and Tioulit canyons; see Fig. 2B). They are up to 60 m high and have a conical shape (Westphal et al., 2012).

2.3. Oceanography

The dominant water masses off Mauritania comprise (i) surface waters in the mixed layer down to 100–150 m water depth, (ii) the North and the South Atlantic Central Waters (NACW, SACW; Fig. 1) representing the upper permanent thermocline waters (down to ~600 m) formed in the North and South Atlantic subtropical gyres, (iii) the Antarctic Intermediate Water (AAIW; 600–1000 m), and (iv) the North Atlantic Deep Water (1000–1600 m; Pastor et al., 2012; Stramma et al., 2005; Zenk et al., 1991). The Mauritanian coral mound province occurring south of 21°N and at intermediate water depths is today mainly influenced by the SACW. The SACW is carried northward by the along-slope Poleward Undercurrent (PUC; Fig. 1; Barton, 1989; Pelegrí et al., 2017). The PUC is a relatively narrow (30→40 km wide) slope current with maximum speeds of ~0.25 m s^{-1}, and represents the predominant current between 100 m and 300 m water depth (Pelegrí et al., 2017; Peña→Izquierdo et al., 2012). The northward transport of SACW is enhanced during summer and autumn, when the (surface) Mauritanian Current develops as a coastal component of the North Equatorial Countercurrent between Cap Vert and Cap Blanc (Fig. 1; Arístegui et al., 2009; Mittelstaedt, 1983; Pelegrí et al., 2017; Stramma and Schott, 1999). North of the Mauritanian coral mound province, the relatively cold and fresh SACW is separated from the comparatively warm and saline NACW by the Cape Verde frontal zone (CVFZ), which is tilted from 21°N (off Cap Blanc) to ~16°N (Cap Verde islands; Fig. 1; Peña-Izquierdo et al., 2015; Tomczak, 1984; Zenk et al., 1991). The NACW is carried southward

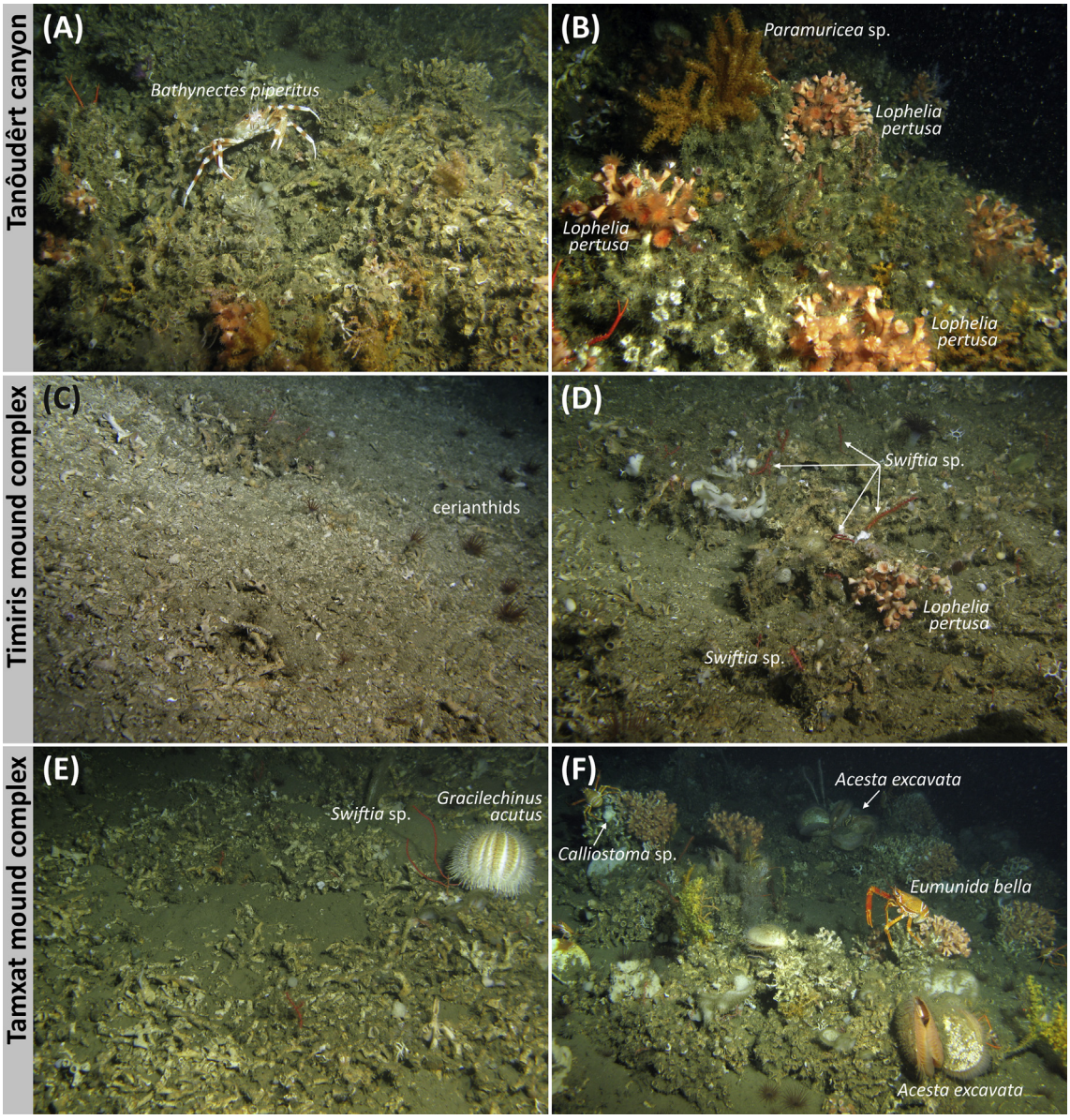

Fig. 3. ROV images (copyright Tomas Lundälv, Sven Lovén Centre, University of Gothenburg) recorded during R/V Maria S. Merian cruise MSM16-3 showing the recent occurrence of fossil and living cold-water corals and associated fauna along the Mauritanian margin (Westphal et al., 2012). **A**: Tanôudêrt canyon, 562 m water depth. Massive reefal coral framework covered by a dense "turf" layer dominated by tube-building amphipods, hydroids, branched and anastomosing foraminifers. Some alive *Lophelia pertusa* colony branches are present. The associated fauna comprises octocorals, encrusting sponges, squad lobster and *Bathynectes piperitus*. **B**: Tanôudêrt canyon, 546 m depth. Reefal coral framework forming a fringe near the base of the coral mound developed on top of the canyon. The exposed fossil framework is covered by a dense turf layer. Many live *L. pertusa* colonies are present. Other fauna comprises several octocorals, some solitary corals, sponges, and squad lobster. **C**: Mid-slope on a deep Timiris coral mound, 532 m depth. Fossil coral rubble speckled with cerianthids and octocorals. **D**: Mid-slope on a deep Timiris coral mound, 557 m depth. A living *Lophelia*-colony attached to a fossil coral skeleton of 12.5 ka in age (ROV-sample GeoB 14873-3; see Tables 1 and 2). Other fauna consists of octocorals, sponges, ascidians, bryozoans and cerianthids. **E**: Characteristic coral rubble surface on a deep Tamxat coral mound, 499 m depth. The associated fauna consists of sponges, caryophylliid solitary corals, bryozoans and hydroids together with some decapods. **F**: Near the summit of a deep Tamxat coral mound, 502 m depth. Exposed *L. pertusa* coral framework (20–30 cm high) with live *L. pertusa* colonies. Framework-attached fauna comprises octocorals, sponges, bryozoans, hydroids and *Acesta excavata*. The mobile fauna shows squat lobster (*Eumunida bella*), ophiuroids and gastropods. Soft sediment substrate beneath the framework provides habitat for a rich sediment-dwelling community (cerianthids, foraminifers, polychaetes).

by the Canary Current (CC), which flows on the NW African outer shelf and upper slope and forms the eastern branch of the North Atlantic subtropical gyre (Fig. 1). North of Cap Blanc, the dominant fraction of the CC detaches from the NW African margin and gradually turns into the wind-driven North Equatorial Current (Mittelstaedt, 1991). The SACW has a higher nutrient content and lower DOCs compared to the NACW (Minas et al., 1982; Stramma et al., 2005). Recent oceanographic studies further distinguish between an upper (uSACW; above 300 m) and a lower core (lSACW; below 300 m) of the SACW with the uSACW being characterized by higher DOCs compared to the lSACW (Pastor et al., 2012; Peña-Izquierdo et al., 2015). Within the lSACW, the nutrient content increases with depth, while DOCs concurrently decrease (Pelegrí et al., 2017). Below the lSACW flows the AAIW in a northward direction (Stramma et al., 2005). Within the AAIW, the nutrient content continues to increase until maximum values are reached at 700–800 m water depth, and DOCs return to moderate but still low values (Pelegrí et al., 2017; Peña-Izquierdo et al., 2015).

A well-developed OMZ exists in the depth range of the lSACW and the upper AAIW (~300–700 m water depth), extending latitudinally from about 20°N to 5°N (Karstensen et al., 2008; Stramma et al., 2008). Lowest DOCs of 1.0–1.3 ml l^{-1} were measured between 400 m and 550 m water depth (Pelegrí et al., 2017; Peña-Izquierdo et al., 2015; Ramos et al., 2017), which exactly matches the depth level of coral mound occurrence. The OMZ is regulated by the upwelling-induced high ocean surface productivity, and the subsequent increased export of organic matter, which consumes oxygen through its degradation. The Mauritanian margin belongs to the most important eastern boundary upwelling areas worldwide (Behrenfeld and Falkowski, 1997; Carr and Kearns, 2003). Permanent upwelling occurs north of Cap Blanc, while seasonal upwelling prevails south of 21°N fed by the SACW (Arístegui et al., 2009; Mittelstaedt, 1991; Nykjær and Van Camp, 1994; Pastor et al., 2008). The upwelling of nutrient-rich central waters and the resulting high productivity occurs predominantly within a narrow strip (10–20 km) and is concentrated along the outer shelf and upper slope (Mittelstaedt, 1991). A pronounced and seasonally persistent nepheloid layer occurs at the depth of the OMZ between 400 and 800 m (Fischer et al., 2009). This layer contains high amounts of particulate organic matter, which is advected laterally along the isopycnal between the SACW and the AAIW over more than 600 km distance offshore from its source at the shelf (Arístegui et al., 2009; Karakas et al., 2006).

3. Material and methods

3.1. Sampling of cold-water corals

During R/V MARIA S. MERIAN expedition MSM16-3 in 2010, surface samples and sediment cores were collected along the Mauritanian margin (Westphal et al., 2012). The entire sampling area stretches over a latitudinal distance of >300 km from 20°15′N to 17°29′N (Fig. 2) and covers a water depth range between 415 and 620 m (Table 1). Sampling targets comprised upper canyon flanks (Tanôudêrt, Nouamghar, Inchiri, and Tioulit canyons), coral mounds developed on canyon flanks (Tanôudêrt and Tioulit canyons) and coral mounds of the Timiris, Banda and Tamxat mound complexes along the southern Mauritanian slope (Fig. 2).

Surface coral samples were collected by a grab sampler, a giant box corer, and by the remotely operated vehicle (ROV) Sperre SubFighter 7500 DC (Sven Lovén Centre for Marine Sciences Tjarno, University of Gothenburg, Sweden; Westphal et al., 2012). The surface samples were complemented by the collection of six gravity cores, which had recoveries between 3.6 m and 10.3 m and were retrieved from the top of coral mounds (Table 1, Fig. 2). All cores display an impressive dominance of the scleractinian coral *L. pertusa*, while other CWC species are rare, and exhibit a consistent association with large shells of the file clam *Acesta excavata* and bryozoans (Fig. 4). The coral/shell fragments are embedded in olive grey to dark grey silty matrix sediments (Fig. 4). Pristine fragments of *L. pertusa* were sampled for Uranium-series dating from each surface samples and from all sediment cores at different core depths (Table 1).

3.2. U/Th age determination on cold-water coral fragments

In total, 77 well-preserved and pristine fragments of *L. pertusa* were used for Uranium-series dating. The measurements were conducted at the Laboratory for Climate and Environmental Sciences (LSCE) at Gif-sur-Yvette, France, and at the Institute for Environmental Physics at the Heidelberg University (IUP), Germany. For most of the U series isotope analysis a multi-collector inductively coupled plasma mass spectrometer was used at either institute (ThermoFisher Neptune plus; Matos et al., 2015; Wefing et al., 2017). However, in a few cases an inductively coupled plasma source quadrupole mass spectrometer was used (Douville et al., 2010). Prior to analyses, the coral samples were cleaned mechanically to remove any contaminants from the skeleton surface (e.g., epibionts, borings, iron–manganese crusts, coatings) and were then prepared chemically using weak acid leaching and water rinsing according to the procedure described in Frank et al. (2004), recently updated by Wefing et al. (2017). The reproducibility of mass spectrometric measurements was assessed using the international Uranium standard material HU1 (Cheng et al., 2000; Frank et al., 2004; Wefing et al., 2017).

3.3. Data processing

The obtained Mauritanian coral ages (n = 77) were compared with coral ages (n = 21) published in Eisele et al. (2011). Ages originating from submarine canyons and from coral mounds were treated separately. In addition, coral ages obtained from the six sediment cores collected from coral mounds were used to calculate coral mound ARs (reported in cm kyr^{-1}), which provide indispensable information to reconstruct the temporal development of a coral mound. Coral ages obtained from core records often display distinct age clusters (at least consisting of two ages, stratigraphically closely related), which represent periods of sustained CWC growth resulting in enhanced mound ARs (active mound stage). Age gaps between these clusters point to periods of reduced CWC occurrence or a temporary absence of CWCs, which led to a slow-down or stagnation in mound formation expressed in very low ARs, or erosion (dormant mound stage). Whenever the coral ages of a cluster revealed a continuous chronological order, ARs were calculated from age to age thereby providing minimum (AR_{min}) and maximum ARs (AR_{max}) for a distinct cluster. In addition, average ARs ($AR_{ø}$) were estimated for each age cluster. For coral age clusters that exhibit a significant age reversal, an age-to-age AR calculation was not possible. However, in cases the age data did not differ within the uncertainty of the ages, the oldest and youngest coral ages in relation to the maximum and minimum core depths of the respective core interval were used for the calculation of an $AR_{ø}$.

4. Results

4.1. Dating quality and coral age distribution

All CWC fragments indicated minor physico-chemical alteration or dissolution, which may disturb Uranium-series ages. Measured ^{232}Th concentrations are small with <2.5 ppb for 91% of all samples (Table 2). Initial $\delta^{234}U_i$ values are variable and range between 138.6 ± 0.8‰ and 176.0 ± 1.1‰ (Table 2). Ninety-six percent of all samples rely on $\delta^{234}U_i$ values, which plot within a narrow band of ±10‰ compared to the value of modern seawater (146.8‰; Andersen et al., 2010) and can therefore be treated as being reliable. Three samples show high $\delta^{234}U_i$ values of >158‰ (Table 2), and thus are likely influenced by diagenetic alteration.

Calculated Uranium-series ages (given in kiloyears, ka) considering all CWC sampling sites along the Mauritanian margin range from ~193 ± 1.8 ka to modern (0.019 ± 0.008 ka; Table 2). Corals collected from the surface of the upper flanks of the Mauritanian canyons (n = 11) have Late Holocene to recent ages, but are not older than 1.1 ka (Fig. 5). In contrast, CWCs from the Mauritanian coral mounds (n = 66) reveal mostly ages of >11.4 ka, except of one age of 8.7 ka and two recent ages (25 and 94 years), all obtained from surface coral samples (Table 2). All mound-derived coral ages (comprising surface and core samples) show distinct age clusters

Table 1
Metadata of cold-water coral-bearing surface samples (n = 28) collected with a grab sampler (GR), a box corer (BC), and a ROV, and of long sediment cores (n = 6) retrieved with a gravity corer (GC) during R/V MARIA S. MERIAN cruise MSM16-3 (for sample location see also Fig. 1). Sampled cold-water coral sites comprise canyons (C) and coral mounds (M) along the Mauritanian margin. Number of dated *Lophelia pertusa* fragments (dLp) collected from each sample is indicated. Abbreviations: LAT, latitude; LON, longitude; WD, water depth; REC, recovery.

No.	C/M	Sample-ID (GeoB14)	Gear	LAT (N)	LON (W)	WD (m)	REC	dLp	Location
northern sector									
1	C (a)	796–4	ROV	20°14.827′	17°40.182′	−617	surface	1	Tanôudêrt canyon
2	C (a)	796–6	ROV	20°14.796′	17°40.166′	−568	surface	1	Tanôudêrt canyon
3	C (a)	802–1	GR	20°14.791′	17°40.188′	−595	surface	1	Tanôudêrt canyon
4	C (a)	801–1	GR	20°14.762′	17°40.173′	−568	surface	1	Tanôudêrt canyon
5	C (a)	800–1	GR	20°14.748′	17°40.187′	−560	surface	1	Tanôudêrt canyon
6	C (a)	798–2	BC	20°14.699′	17°40.131′	−560	surface	1	Tanôudêrt canyon
7	M (a)	796–7	ROV	20°14.585′	17°40.109′	−500	surface	1	mound developed on Tanôudêrt canyon flank
8	M (a)	799–1	BC	20°14.574′	17°40.088′	−490	surface	1	mound developed on Tanôudêrt canyon flank
9	M (a)	799–2	GC	20°14.575′	17°40.088′	−491	360 cm	8	mound developed on Tanôudêrt canyon flank
10	M (b)	760–2	BC	19°44.292′	17°08.754′	−478	surface	1	mound developed on Arguin canyon flank
11	C (b)	779–3	ROV	19°10.777′	16°48.352′	−618	surface	1	Nouamghar canyon
12	C (c)	871–7	ROV	19°08.351′	16°45.818′	−540	surface	1	Inchiri canyon
southern sector									
13	M (c)	874–7	ROV	18°57.843′	16°51.157′	−446	surface	1	Timiris mound complex, shallow mounds (top)
14	M (c)	882–1	GC	18°57.801′	16°51.166′	−415	266 cm	5	Timiris mound complex, shallow mounds (top)
15	M (c)	880–1	BC	18°57.800′	16°51.169′	−438	surface	1	Timiris mound complex, shallow mounds (top)
16	M (d)	878–1	BC	18°57.934′	16°52.073′	−493	surface	1	Timiris mound complex, deep mounds (top)
17	M (d)	884–1	GC	18°57.803′	16°52.123′	−492	813 cm	9	Timiris mound complex, deep mounds (top)
18	M (d)	877–1	BC	18°57.802′	16°52.126′	−498	surface	1	Timiris mound complex, deep mounds (top)
19	M (d)	876–1	BC	18°57.743′	16°52.244′	−548	surface	1	Timiris mound complex, deep mounds (flank)
20	M (d)	873–3	ROV	18°57.736′	16°52.244′	−557	surface	1	Timiris mound complex, deep mounds (flank)
21	M (d)	873–2	ROV	18°57.725′	16°52.264′	−574	surface	1	Timiris mound complex, deep mounds (flank)
22	C (d)	886–4	ROV	18°39.004′	16°43.589′	−618	surface	1	Tioulit canyon
23	C (d)	886–2	ROV	18°39.003′	16°43.589′	−620	surface	1	Tioulit canyon
24	C (d)	888–1	BC	18°38.997′	16°43.607′	−600	surface	1	Tioulit canyon
25	M (e)	886–6	ROV	18°38.968′	16°43.639′	−583	surface	1	mound developed on Tioulit canyon flank
26	M (f)	898–1	GR	17°40.193′	16°40.415′	−505	surface	1	Banda mound complex (flank)
27	M (f)	897–1	GR	17°40.171′	16°40.483′	−505	surface	1	Banda mound complex (flank)
	M (f)	[a]11569-2	GC	17°40.001′	16°40.327′	−470	509 cm	21	Banda mound complex (flank)
28	M (g)	903–2	GC	17°32.854′	16°39.698′	−415	675 cm	5	Tamxat mound complex, shallow mounds (top)
29	M (g)	903–1	BC	17°32.853′	16°39.700′	−414	surface	1	Tamxat mound complex, shallow mounds (top)
30	M (h)	904–1	BC	17°32.559′	16°39.805′	−510	surface	1	Tamxat mound complex, deep mounds (top)
31	M (h)	904–2	GC	17°32.558′	16°39.806′	−517	1028 cm	15	Tamxat mound complex, deep mounds (top)
32	M (i)	905–2	GC	17°32.456′	16°39.999′	−493	965 cm	7	Tamxat mound complex, deep mounds (top)
33	M (j)	910–2	BC	17°28.998′	16°41.647′	−535	surface	1	Tamxat mound complex
34	M (j)	911–1	BC	17°28.910′	16°41.509′	−450	surface	1	Tamxat mound complex

[a] Coral ages published by Eisele et al., 2011.

(Fig. 5). The oldest (dated) coral is of late Marine Isotope Stage (MIS) 7 age (~192.6 ka) and is followed by a large age gap covering a time span of ~75 kyr. A first cluster of five ages ranges from 117.2 ka to 90.2 ka and coincides with MIS5. A second age cluster consisting of 40 ages ranges between 67.5 ka and 18.7 ka and corresponds to the last glacial (MIS 4-2). Overall, 61% of all mound-derived coral ages fall into this cold climate period. A distinct age gap is documented between 27.2 ka and 20.9 ka, which mainly encompass the early Last Glacial Maximum (LGM: 25–19 ka; note the LGM and rapid events during the deglaciation are temporally defined according to Gallego-Torres et al., 2014). Upon this age gap follow seven further glacial ages ranging from 20.9 ka to 18.7 ka (Table 2), which correspond to the late LGM. After the LGM, again an age gap encompassing 4.3 kyr is documented, which largely overlaps with the Heinrich event 1 (HE1: 17.5–15.5 ka; Fig. 5). The youngest mound-derived coral age cluster of 16 ages ranges between 14.3 ka and 11.4 ka, encompassing the Bølling-Allerød (BA: 15.5. - 13.5 ka), the Younger Dryas (YD: 13.5–11.5 ka) and the very Early Holocene (<11.5 ka; Table 2, Fig. 5).

4.2. Coral mound aggradation periods and rates

Distinct coral age clusters become more evident when considering the six core records separately (Fig. 6). The northernmost coral mound sampled for this study is located on top of the southern flank of the Tanôudêrt canyon (Fig. 2B). The core retrieved from the mound's top at 491 m water depth reveals two age clusters (Fig. 6). The first cluster ranges from 40.2 ka to 36.5 ka (four ages in continuous chronological order) and plots into MIS3. The corresponding calculated $AR_{ø}$ is 44 cm kyr^{-1} (AR_{min}: 27 cm kyr^{-1}, AR_{max}: 107 cm kyr^{-1}; Table 3). This first age cluster is followed by an age gap of more than 25 kyr. The second age cluster in this core (four ages in discontinuous chronological order, but within dating error) comprises a very narrow time slot of just 68 years at around 11.4 ka (start of the Holocene) and corresponds to a remarkably high $AR_{ø}$ of 1647 cm kyr^{-1}. A surface coral sample collected from the top of the mound at 490 m water depth revealed an age of 8.7 ka (Table 2).

Two cores collected from the Timiris mound complex (Fig. 2C) show very different pattern regarding the coral age distribution. The core collected from the upper mound chain in 415 m water depth shows a single age of 192.6 ka, before one poorly pronounced age cluster between 117.2 ka and 107.9 ka occurs (four ages in discontinuous chronological order), which corresponds to the MIS5. The calculated $AR_{ø}$ is very low with 16 cm kyr^{-1} (Fig. 6, Table 3). These are the oldest coral ages retrieved in the cores from this study. The only other MIS5 age (103.5 ka) is from a surface coral sample (Tables 1 and 2) collected from the same coral mound (Fig. 2C). A second surface coral sample collected from this mound

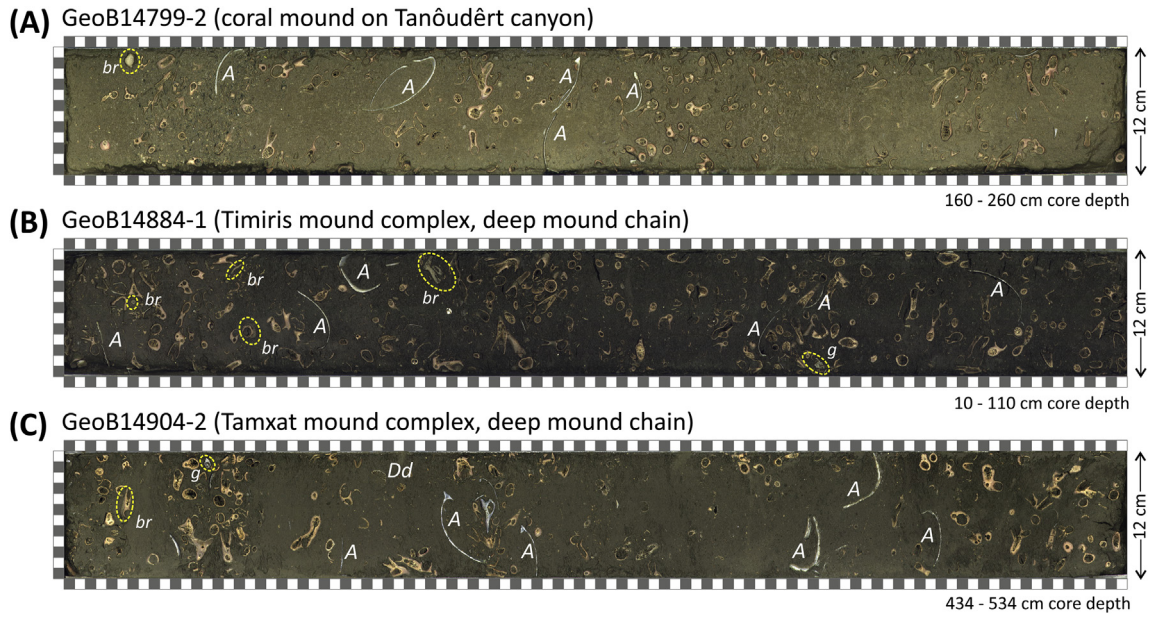

Fig. 4. Images of cold-water coral-bearing sediment cores collected from coral mounds along the Mauritanian margin. (**A**) Core GeoB14799-2 (160–260 cm core depth) collected from a coral mound developed on the Tanôudêrt canyon. (**B**) Core GeoB14884-1 (10–110 cm core depth) collected from a deep mound of the Timiris mound complex. (**C**) Core GeoB14904-2 (434–534 cm core depth) collected from a deep mound of the Tamxat mound complex. All cores shows an outstanding dominance of *Lophelia pertusa* fragments, which are embedded in fine matrix sediments (A: olive grey sandy silt to fine sand, B: very dark grey silt, C: dark olive grey silt). Other shells comprise large shells of the bivalve *Acesta excavata* (*A*), bryozoans (*br*), the solitary coral *Desmophyllum dianthus* (*Dd*), and gastropods (*g*).

shows an age of 55.9 ka (Tables 1 and 2). The core collected from a mound of the lower Timiris mound chain in 492 m water depth reveals one age cluster between 58.8 ka and 36.6 ka (eight ages in discontinuous chronological order, but within dating error) that largely covers the MIS3. Calculated $AR_{ø}$ is 32 cm kyr^{-1} (Fig. 6, Table 3). A coral collected from the top of this core has an age of 19.8 ka, hence between 36.6 ka and 19.8 ka, the $AR_{ø}$ decreased to 6 cm kyr^{-1} (Table 3).

Three sediment cores were collected from mounds belonging to the Tamxat mound complex (Fig. 2E). The core retrieved from the upper mound chain at 415 m water depth reveals just one coral age cluster during the MIS3 ranging from 53.6 ka to 41 ka (five ages in continuous chronological order) and corresponding to an $AR_{ø}$ of 52 cm kyr^{-1} (AR_{min}: 24 cm kyr^{-1}, AR_{max}: 478 cm kyr^{-1}; Fig. 6, Table 3). A surface coral sample collected from the top of the same mound at 414 m depth also shows a MIS3 age of 43.1 ka (Tables 1 and 2). Two cores from the lower mound chain of the Tamxat mound complex reveal several age clusters corresponding to the largest $AR_{ø}$ obtained for all studied Mauritanian coral mounds (Fig. 6, Table 3). The core collected from 493 m water depth shows two distinct age clusters. One cluster, although just comprising two coral ages, ranges from 36.9 ka to 34.8 ka and coincides with the MIS3. The calculated $AR_{ø}$ is 101 cm kyr^{-1} (Table 3). A second cluster between 14.3 ka and 13.1 ka is restricted to the BA (three ages) and very early YD (one age), for which remarkable 4.3 m of mound sediments were deposited in just 1.2 kyr. The chronological order of these ages allows an age-to-age calculation of the AR, which varies between 160 cm kyr^{-1} and 1156 cm kyr^{-1} ($AR_{ø}$: 364 cm kyr^{-1}; Table 3). Between both age clusters, a period of reduced $AR_{ø}$ of 15 cm kyr^{-1} lasted for ~21 kyr, just one coral age of 20.9 ka falls into this interval. The second core collected from the lower mound chain at 517 m water depth contains three coral age clusters. The first one ranges from 31.1 ka to 27.2 ka (six ages in continuous chronological order, despite of one outlier age not considered for AR calculation), thus encompassing the transition from the MIS 3 to the MIS2. Calculated $AR_{ø}$ is 114 cm kyr^{-1} (AR_{min}: 64 cm kyr^{-1}, AR_{max}: 429 cm kyr^{-1}; Fig. 6, Table 3). Following an age gap lasting for 7.4 kyr, a second cluster (five ages in discontinuous chronological order, but within dating error) with a very narrow age range of 19.8 ka to 18.7 ka occurs. During this time interval in the late LGM, 2.2 m of mound sediments were deposited within 1.1 kyr corresponding to an $AR_{ø}$ of 192 cm kyr^{-1} (Table 3). The following age gap lasted for 4.6 kyr. The youngest documented age cluster ranges from 14.0 ka to 12.5 ka and is restricted to the BA (two ages) and the YD (one age). $AR_{ø}$ is 88 cm kyr^{-1}, while AR_{min} and AR_{max} vary significantly between 46 cm kyr^{-1} and 1667 cm kyr^{-1}, respectively (Fig. 6, Table 3). A surface coral sample collected from the same mound and at the same depth level of 510 m also reveals a BA-age of 13.8 ka (Tables 1 and 2).

5. Discussion

CWCs are widely distributed along the entire Mauritanian margin occurring on the 400-km-long coral mound chains but also within the numerous submarine canyons (Colman et al., 2005; Ramos et al., 2017; Westphal et al., 2012). While the living coral population shows today a rather sparse occurrence (Fig. 3; Colman et al., 2005; Westphal et al., 2012), the widespread and massive deposits of fossil corals and the development of such an impressively vast coral mound area point to a far more successful proliferation of CWCs in the past. Up to this study, the knowledge about the timing of CWC growth along the Mauritanian margin was limited, based on one core record obtained from the Banda mound complex (see Fig. 2D). This local study revealed two last glacial age clusters ranging from 65.4 ka to 57.4 ka and from 45.2 ka to 32.3 ka, and one single age of 14.2 ka (Eisele et al., 2011). Our study substantially improves the database of and the understanding about the temporal and spatial occurrence of CWCs along the Mauritanian margin by considering coral material obtained from an extended latitudinal transect (Fig. 2) and by providing a coral age dataset that covers the past 193 ka (Table 2). Overall, four major periods of past CWC occurrence were identified that coincide with the MIS5

Table 2
Cold-water coral ages, isotope concentration and ratios. All U-series datings were obtained from *Lophelia pertusa* (see Table 1 for site and sample information).

N	Sample-ID (GeoB14)	S	SD (cm)	Labcode	Age (ka BP)	±	^{238}U (ppm)	±	^{232}Th (ppb)	±	$\delta^{234}U_m$ (‰)	±	$\delta^{234}U_i$ (‰)	±	R
1	**2**	**3**	**4**	**5**	**6**		**7**		**8**		**9**		**10**		**11**
Tanoudêrt canyon area															
1	796–4	C (a)	0	GIF-2442	**0.153**	0.051	3.7621	0.0347	1.1583	0.0263	148.0	2.2	148.1	2.2	R
2	796–6	C (a)	0	GIF-2443	**0.037**	0.037	3.2525	0.0047	0.7328	0.0027	146.5	1.8	146.5	1.8	R
3	802–1	C (a)	0	GIF-2441	**0.067**	0.065	2.8593	0.0043	0.2376	0.0016	147.8	1.2	147.8	1.2	R
4	801–1	C (a)	0	GIF-2440	**0.405**	0.094	3.0794	0.0045	0.4268	0.0033	147.6	1.0	147.8	1.0	R
5	800–1	C (a)	0	GIF-2439	**1.127**	0.103	3.3155	0.0060	0.3031	0.0023	146.8	1.1	147.3	1.1	R
6	798–2	C (a)	0	GIF-2437	**0.157**	0.061	3.8730	0.0062	0.4543	0.0010	147.5	1.3	147.5	1.3	R
7	796–7	M (a)	0	GIF-2444	**0.094**	0.094	3.7793	0.0218	1.1111	0.0092	143.7	2.9	143.7	2.9	R
8	799–1	M (a)	0	GIF-2438	**8.685**	0.229	4.8972	0.0067	2.0702	0.0021	147.3	7.1	151.0	7.3	R
9	799–2	M (a)	4	GIF-2785	**11.443**	0.041	3.6976	0.0021	0.2723	0.0002	140.8	1.2	145.4	1.3	R
10	799–2	M (a)	51	GIF-2786	**11.375**	0.028	3.5341	0.0016	0.3674	0.0001	144.2	0.8	149.0	0.8	R
11	799–2	M (a)	95	GIF-2787	**11.414**	0.036	3.1205	0.0011	0.5247	0.0004	143.0	0.9	147.6	0.9	R
12	799–2	M (a)	116	GIF-2788	**11.408**	0.043	3.5198	0.0014	0.3432	0.0002	143.3	1.2	148.0	1.3	R
13	799–2	M (a)	181	GIF-2792	**36.505**	0.081	3.7999	0.0014	0.4779	0.0002	133.9	1.1	148.4	1.3	R
14	799–2	M (a)	237	GIF-2791	**38.578**	0.064	3.3701	0.0016	0.3000	0.0002	138.1	0.7	154.0	0.7	R
15	799–2	M (a)	288	GIF-2790	**39.055**	0.072	3.3032	0.0018	0.1340	0.0001	140.1	0.5	156.4	0.6	R
16	799–2	M (a)	341	GIF-2789	**40.163**	0.115	3.4467	0.0014	0.2386	0.0002	145.4	1.2	162.9	1.3	NR
Arguin canyon area															
17	760–2	M (b)	0	GIF-2445	**49.099**	0.366	3.2875	0.0048	0.5994	0.0012	128.5	1.0	147.7	1.1	R
Timiris canyon area															
18	779–3	C (b)	0	GIF-2446	**0.073**	0.073	4.0471	0.0054	1.5934	0.0023	146.8	1.3	146.9	1.3	R
19	871–7	C (c)	0	GIF-2447	**0.852**	0.032	3.9104	0.0122	0.2716	0.0022	145.9	1.2	146.3	1.2	R
Timiris mound complex															
20	874–7	M (c)	0	GIF-2455	**55.894**	0.249	3.3125	0.0016	2.0384	0.0057	130.4	0.8	152.7	0.9	R
21	882–1	M (c)	7	IUP-8220	**107.900**	0.49	3.2870	0.0002	1.0707	0.0027	111.6	0.8	151.4	1.1	R
22	882–1	M (c)	93	IUP-8221	**115.530**	0.63	2.8134	0.0002	0.5451	0.0017	111.3	1.1	154.3	1.5	R
23	882–1	M (c)	111	IUP-8222	**117.160**	0.57	2.5292	0.0001	1.1608	0.0024	108.1	1.3	150.5	1.8	R
24	882–1	M (c)	159	IUP-8223	**114.230**	0.57	3.0729	0.0002	2.7124	0.0049	110.1	1.2	152.0	1.7	R
25	882–1	M (c)	262	IUP-8224	**192.600**	1.8	2.7485	0.0002	2.6264	0.0070	88.0	1.4	151.6	2.6	R
26	880–1	M (c)	0	GIF-2453	**103.464**	0.383	3.2677	0.0052	3.7927	0.0061	114.3	1.0	153.2	1.3	R
27	878–1	M (d)	0	GIF-2450	**11.509**	0.043	3.2706	0.0021	2.2456	0.0029	145.0	0.6	149.8	0.6	R
28	884–1	M (d)	19	IUP-8052	**19.803**	0.069	3.6488	0.0002	0.4405	0.0012	136.7	0.7	144.6	0.7	R
29	884–1	M (d)	99	IUP-8053	**36.710**	0.1	4.6413	0.0002	1.0520	0.0021	126.8	0.6	140.7	0.7	R
30	884–1	M (d)	119	IUP-8054	**36.570**	0.11	2.9335	0.0001	1.1201	0.0018	133.3	1.1	147.8	1.3	R
31	884–1	M (d)	288	IUP-8055	**41.940**	0.15	3.5069	0.0001	2.4291	0.0053	127.1	0.5	143.1	0.5	R
32	884–1	M (d)	317	IUP-8056	**40.150**	0.14	2.9823	0.0001	1.3436	0.0028	129.1	0.6	144.6	0.7	R
33	884–1	M (d)	437	IUP-8057	**46.990**	0.19	2.6194	0.0001	1.2930	0.0034	132.2	0.6	151.0	0.7	R
34	884–1	M (d)	458	IUP-8058	**46.550**	0.17	3.1019	0.0001	0.8726	0.0023	128.4	0.5	146.4	0.6	R
35	884–1	M (d)	638	IUP-8059	**53.650**	0.18	2.8601	0.0001	0.7109	0.0018	123.3	0.8	143.4	0.9	R
36	884–1	M (d)	806	IUP-8060	**58.830**	0.27	2.2793	0.0001	1.2857	0.0034	118.7	0.7	140.2	0.8	R
37	877–1	M (d)	0	GIF-2449	**13.180**	0.063	3.2740	0.0025	0.9870	0.0029	145.3	0.9	150.8	0.9	R
38	876–1	M (d)	0	GIF-2448	**67.525**	0.695	3.6416	0.0061	2.0140	0.0030	131.0	1.1	158.7	1.3	NR
39	873–3	M (d)	0	GIF-2452	**12.533**	0.044	3.0871	0.0018	0.6314	0.0010	145.1	1.0	150.3	1.0	R
40	873–2	M (d)	0	GIF-2451	**42.826**	0.133	4.1236	0.0030	1.4438	0.0020	136.2	0.6	153.8	0.6	R
Tioulit canyon area															
41	886–4	C (d)	0	GIF-2458	**0.019**	0.008	3.2897	0.0025	1.3967	0.0036	149.0	0.6	149.0	0.6	R
42	886–2	C (d)	0	GIF-2457	**0.029**	0.007	2.9242	0.0027	0.5970	0.0014	146.9	0.9	146.9	0.9	R
43	888–1	C (d)	0	GIF-2456	**0.483**	0.006	3.6523	0.0032	0.4697	0.0007	145.7	1.0	145.9	1.0	R
44	886–6	M (e)	0	GIF-2459	**0.025**	0.004	3.5199	0.0040	0.6143	0.0010	145.8	1.3	145.8	1.3	R
Banda mound complex															
45	898–1	M (f)	0	GIF-2462	**28.719**	0.141	3.1779	0.0061	0.5410	0.0010	134.2	2.4	145.6	2.6	R
46	897–1	M (f)	0	GIF-2461	**12.838**	0.032	3.2471	0.0031	0.3361	0.0003	144.9	0.7	150.3	0.8	R
Tamxat mound complex															
47	903–2	M (g)	6	IUP-8225	**40.960**	0.15	2.9527	0.0002	1.1104	0.0027	126.99	0.91	142.6	1.0	R
48	903–2	M (g)	144	IUP-8226	**46.780**	0.18	2.7879	0.0002	1.1426	0.0031	124.68	0.99	142.3	1.1	R
49	903–2	M (g)	297	IUP-8227	**47.100**	0.15	3.0452	0.0002	0.9093	0.0021	123.08	0.96	140.6	1.1	R
50	903–2	M (g)	459	IUP-8228	**51.910**	0.22	3.2434	0.0002	1.6057	0.0043	120.64	0.93	139.7	1.1	R
51	903–2	M (g)	672	IUP-8229	**53.600**	0.16	3.1780	0.0002	0.8435	0.0017	119.10	0.71	138.6	0.8	R
52	903–1	M (g)	0	GIF-2463	**43.130**	0.319	3.8915	0.0084	4.8894	0.0226	130.2	1.2	147.1	1.4	R
53	904–1	M (h)	0	GIF-2464	**13.774**	0.075	3.6900	0.0088	2.0933	0.0064	141.8	1.6	147.4	1.7	R
54	904–2	M (h)	1	GIF-2793	**12.525**	0.05	3.4929	0.0012	1.0215	0.0004	143.9	0.9	149.0	1.0	R
55	904–2	M (h)	67	GIF-2795	**13.974**	0.071	3.0501	0.0047	1.1129	0.0014	146.9	1.2	152.9	1.2	R
56	904–2	M (h)	132	GIF-2796	**14.013**	0.066	2.5547	0.0063	0.5274	0.0009	143.7	1.3	149.6	1.3	R
57	904–2	M (h)	216	GIF-2797	**18.786**	0.075	3.1437	0.0067	0.3532	0.0005	139.9	1.5	147.6	1.6	R
58	904–2	M (h)	245	GIF-2798	**19.297**	0.095	2.5036	0.0058	0.5778	0.0008	140.2	1.0	148.1	1.1	R
59	904–2	M (h)	293	GIF-2799	**18.654**	0.085	2.3961	0.0034	0.5340	0.0011	138.4	1.6	145.9	1.7	R
60	904–2	M (h)	356	GIF-2800	**18.820**	0.103	2.7952	0.0066	1.1817	0.0016	139.6	1.0	147.4	1.1	R
61	904–2	M (h)	435	GIF-2801	**19.794**	0.095	2.8955	0.0062	0.8482	0.0011	138.3	1.5	146.3	1.5	R
62	904–2	M (h)	550	GIF-2802	**27.209**	0.13	3.0216	0.0084	0.7993	0.0017	134.6	1.1	145.4	1.2	R

(*continued on next page*)

Table 2 (*continued*)

N	Sample-ID (GeoB14)	S	SD (cm)	Labcode	Age (ka BP)	±	^{238}U (ppm)	±	^{232}Th (ppb)	±	$\delta^{234}U_m$ (‰)	±	$\delta^{234}U_i$ (‰)	±	R
1	**2**	**3**	**4**	**5**	**6**		**7**		**8**		**9**		**10**		**11**
63	904–2	M (h)	622	GIF-2803	**27.377**	0.12	2.4886	0.0057	0.9800	0.0016	131.9	1.2	142.6	1.3	R
64	904–2	M (h)	708	GIF-2804	**27.781**	0.139	2.4507	0.0051	0.5885	0.0012	129.8	1.8	140.5	1.9	R
65	904–2	M (h)	785	GIF-2805	**29.006**	0.144	2.5230	0.0059	0.3898	0.0007	131.3	1.9	142.5	2.1	R
66	904–2	M (h)	856	GIF-2806	**30.109**	0.143	2.9342	0.0063	0.9333	0.0017	129.0	1.2	140.5	1.3	R
67	904–2	M (h)	888	GIF-2807	**32.711**	0.269	2.9552	0.0055	3.3584	0.0060	130.4	2.5	143.3	2.7	R
68	904–2	M (h)	989	GIF-2809	**31.051**	0.143	2.6656	0.0046	0.5863	0.0010	127.3	1.6	139.0	1.8	R
69	905–2	M (i)	1	IUP-8230	**13.130**	0.063	3.1965	0.0002	0.7544	0.0021	140.7	0.9	146.0	0.9	R
70	905–2	M (i)	199	IUP-8231	**13.667**	0.071	3.0891	0.0001	1.1115	0.0027	141.9	1.0	147.5	1.0	R
71	905–2	M (i)	281	IUP-8232	**14.178**	0.087	2.4311	0.0001	1.1516	0.0033	144.0	1.1	149.8	1.2	R
72	905–2	M (i)	429	IUP-8233	**14.306**	0.058	3.0885	0.0002	0.4817	0.0013	139.4	1.2	145.2	1.2	R
73	905–2	M (i)	591	IUP-8235	**20.880**	0.11	2.7974	0.0001	1.1487	0.0039	136.3	1.3	144.5	1.4	R
74	905–2	M (i)	741	IUP-8236	**34.780**	0.25	2.4841	0.0001	3.4650	0.0120	134.3	1.2	148.1	1.4	R
75	905–2	M (i)	953	IUP-8237	**36.880**	0.14	2.8230	0.0002	1.0141	0.0028	126.1	0.9	140.0	1.0	R
76	910–2	M (j)	0	GIF-2465	**90.230**	0.371	3.4626	0.0045	3.4588	0.0097	136.3	0.8	176.0	1.1	NR
77	911–1	M (j)	0	GIF-2466	**55.574**	0.265	3.5007	0.0048	7.0224	0.0122	121.6	1.3	142.4	1.6	R

Column **1**: Number of dated *Lophelia* fragment. **2**: Sample ID: GeoB 14xxx-x. **3**: Sampled seabed structure (S), C: canyon, M: coral mound (see Fig. 2 for letter code). Column **4**: Sampling depth (SD). Column **5**: Labcode. Column **6**: Calculated coral ages. Column **7**: ^{238}U concentration. Column **8**: ^{232}Th concentration. Column **9**: Measured $^{234}U/^{238}U$ activity ratios ($\delta^{234}U_m$) are presented as deviation permil (‰) from the equilibrium value. Column **10**: Decay corrected $^{234}U/^{238}U$ activity ratios ($\delta^{234}U_{initial}$) are calculated from the given ages and with $\lambda_{234}U$: 2.8263 × 10^{-6} yr^{-1}. Column **11**: $\delta^{234}U_i$ criterion and U-Th age quality code. Ages are reliable (R) having values of 146.8‰ (modern seawater) ±10‰, and not reliable (NR; due to potential diagenetic overprint) with values >146.8 ± 10‰ (Andersen et al., 2010).

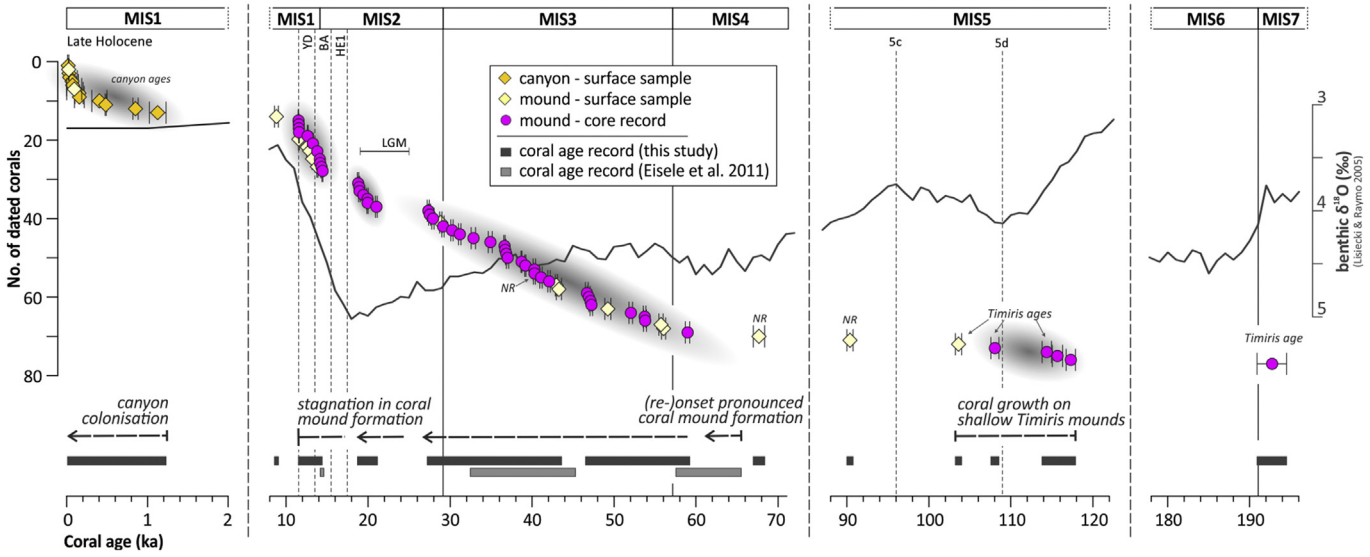

Fig. 5. U-series datings obtained from *Lophelia pertusa* (n = 77; displayed in chronological order) collected from various sites along the Mauritanian margin (note the x-axis breaks between 178 and 122 ka, 88 - 71 ka, and 8 - 2 ka, marked by bold dashed lines). The samples originate from canyon flanks (n = 11; orange diamonds) and from coral mounds, the latter comprising surface samples (n = 17; yellow diamonds) and core samples (n = 49; pink dots). Distinct age clusters are highlighted by grey ovals. Time intervals of coral age clusters identified in the Banda mound complex and published in Eisele et al. (2011) are shown as light grey bars and are compared to the data of this study (dark grey bars). Boundaries between Marine Isotopes Stages (MIS) 1–7 are based on "LR04 Global Pliocene-Pleistocene benthic $\delta^{18}O$ stack" (displayed as bold grey graph) by Lisiecki and Raymo (2005). The Younger Dryas (YD), Bølling-Allerød (BA), Heinrich Event 1 (HE1), and Last Glacial Maximum (LGM) are temporally defined according to Gallego-Torres et al. (2014). (For interpretation of the references to colour in this figure legend, the reader is referred to the Web version of this article.)

(117.2–103.5 ka), the last glacial (MIS4-2, 67.5–18.7 ka), the last deglaciation until the onset of the Early Holocene (14.3–11.4 ka), and the Late Holocene (1.1 ka until today; Fig. 5). This dataset combined with the previously published coral ages (Eisele et al., 2011) clearly documents the almost continuous presence of corals along the entire Mauritanian margin during the last glacial period with yet only two remaining (short-term) interruptions corresponding to the early LGM and to the HE1 (Fig. 5). Nevertheless, as coral ages also correspond to deglacial (BA and YD) and interglacial (MIS5 and Holocene) conditions, it becomes apparent that the previously suggested strict glacial-interglacial contrast of CWC growth off Mauritania (Eisele et al., 2011) documents a general pattern, but must be refined in light of sparse occurrences of CWCs also during interglacial periods.

One aspect that needs to be considered when interpreting coral ages, is a detailed habitat information (see Wienberg and Titschack, 2017). Consequently, for the Mauritanian coral area it is important to differentiate between CWCs collected from the submarine canyons and from the coral mounds along the open slope as both habitats potentially exhibit differing environmental boundary conditions. The available age dataset indeed reveals a striking difference when considering canyon- and mound-derived coral ages separately. All CWCs collected from the canyons show exclusively Late Holocene ages (Fig. 5, Table 2), while CWCs collected from the

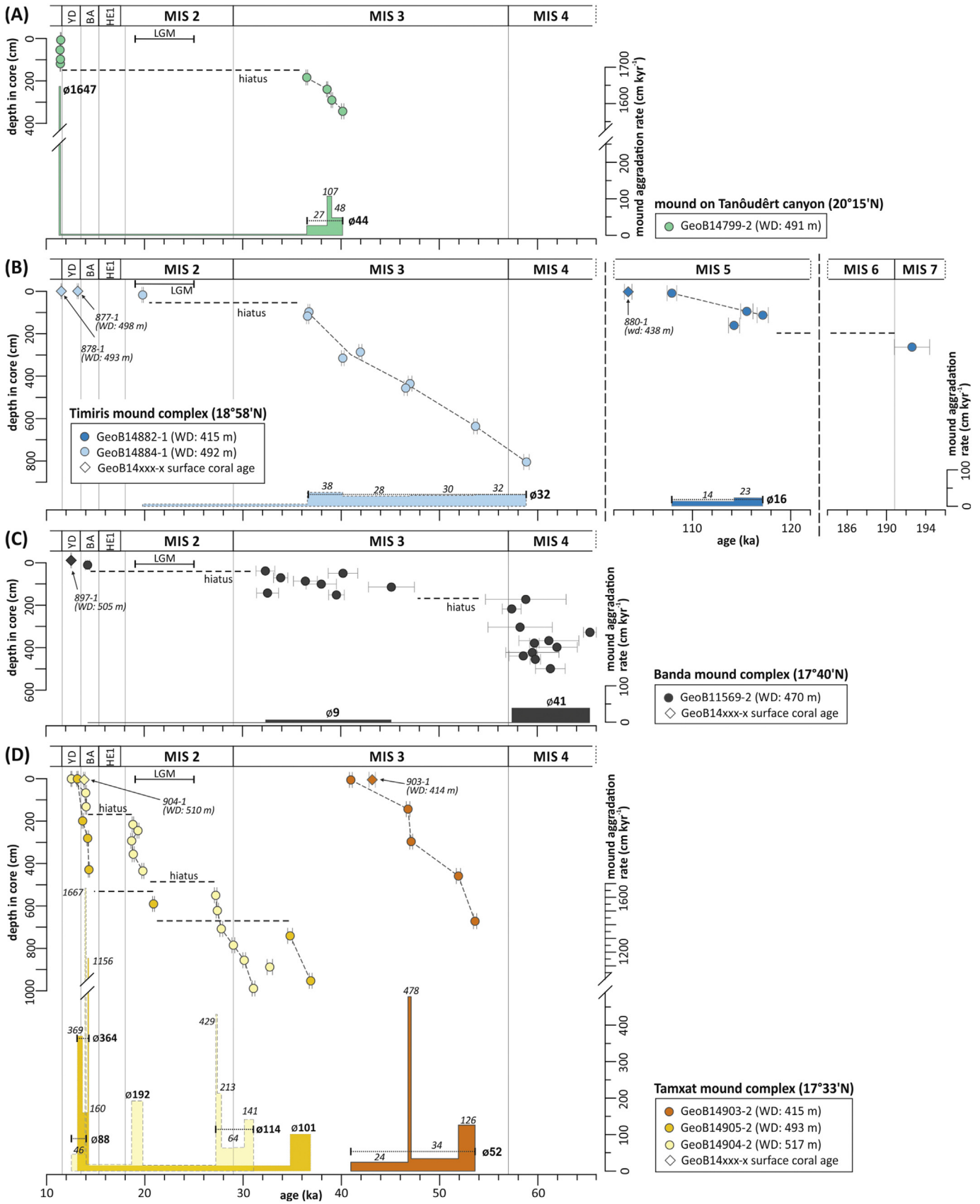

Fig. 6. Coral ages (dots) versus core depth and corresponding calculated coral mound aggradation rates (AR; bold numbers: average AR for a defined aggradation period; italic numbers: AR calculated for two consecutive coral ages). Cores were collected from (**A**) a coral mound developed on the Tanôudêrt canyon, and from mounds belonging to (**B**) the Timiris mound complex (note the x-axis breaks between 66 - 102 ka and 122–184 ka, marked by bold dashed lines), (**C**) the Banda mound complex (data published by Eisele et al., 2011), and (**D**) the Tamxat mound complex. Surface coral ages (diamonds) collected from the same mounds are also displayed, the respective sample-IDs (GeoB14 xxx-x) are indicated. YD: Younger Dryas, BA: Bølling-Allerød, HE1: Heinrich event 1, LGM: Last Glacial Maximum, MIS: Marine Isotope Stage, WD: water depth.

Table 3
Average mound aggradation rates ($AR_ø$; when available minimum and maximum ARs are given in brackets) calculated for core records obtained from coral mounds of the Tanôudêrt canyon area and the Timiris, Banda, and Tamxat mound complexes (note: ARs for core GeoB11569-1 are re-calculated from original data published by Eisele et al., 2011; see Fig. 2 for core location). All cores show distinct coral age clusters (at least consisting of two ages, stratigraphically closely related; number of ages per cluster is given below cluster age range). The clusters are interrupted by periods with apparent age gaps that last for 5–75 kyr and indicate a temporary slow-down in mound formation (dormant mound state). WD: water depth, DUR: duration.

Location	Core-ID	WD	Age cluster 1		Age gap		Age cluster 2		Age gap		Age cluster 3	
			Range	$AR_ø$	DUR	$AR_ø$	Range	$AR_ø$	DUR	$AR_ø$	Range	$AR_ø$
	(GeoB)	(m)	(ka)	(cm kyr^{-1})	(kyr)	(cm kyr^{-1})	(ka)	(cm kyr^{-1})	(kyr)	(cm kyr^{-1})	(ka)	(cm kyr^{-1})
Tanôudêrt area	14799–2	491	40.2–36.5 (4 ages)	44 (27/107)	25.1	3	11.44–11.38 (4 ages)	1647				
Timiris mounds	14882–1 (upper chain)	415	[a]*192.6*		75.4	1	117.2–107.9 (4 ages)	16 (14/23)				
	14884–1 (lower chain)	492	58.8–36.6 (8 ages)	32 (28/38)	16.9	6	[a]*19.8*					
Banda mounds	11569–1	470	65.4–57.4 (11 ages)	41	12.2	2	45.2–32.3 (8 ages)	9	18.0	2	[a]*14.2*	
Tamxat mounds	14903–2 (upper chain)	415	53.6–41.0 (5 ages)	52 (24/478)								
	14905–2 (lower chain)	493	36.9–34.8 (2 ages)	101	°20.5	15	14.3–13.1 (4 ages)	364 (160/1156)				
	14904–2 (lower chain)	517	31.1–27.2 (7 ages)	114 (64/429)	7.4	16	19.8–18.7 (5 ages)	192	4.6	18	14.0–12.5 (3 ages)	88 (46/1667)

[a] Single coral age; °note: one single coral age of 20.9 ka falls into this period.

coral mounds reveal mainly pre-Holocene ages. Only a very recent re-colonisation of the coral mounds can be inferred from the two recent coral ages of 25 and 94 years (Table 2) supplemented by video-observations (Fig. 3; Westphal et al., 2012). This indicates that CWCs were largely absent from the mounds along the open slope and mound formation ceased already with the onset of the Early Holocene.

5.1. Environmental conditions for limited present-day cold-water coral growth

The Mauritanian margin belongs to the most important upwelling areas worldwide that induces high surface primary productivity with maximum seasonal mean values of up to 6 g C m^{-2} day^{-1} (Behrenfeld and Falkowski, 1997; Carr and Kearns, 2003). Thus, at first glance, CWCs should benefit from such highly productive conditions. However, the Mauritanian coral mounds are today bathed by the oxygen-depleted lSACW in exactly the depth level (400–550 m water depth) of the lowest DOCs (1.0–1.3 ml l^{-1}; Ramos et al., 2017) within the OMZ (Figs. 1 and 7). These oxygen concentrations are far below values reported for sustained growth of *L. pertusa* in other areas of the Atlantic (SE US margin: 2.1–2.2 ml l^{-1}, Brooke and Ross, 2014; Gulf of Mexico: 2.6. – 2.7 ml l^{-1}, Davies et al., 2010). Nevertheless, the presence of few living CWCs on the mounds indicates that they may tolerate and (temporarily) survive very low oxygen concentrations. However, their normal aerobic function is likely impaired below ~3.3 ml l^{-1} (at 9 °C water temperature; Dodds et al., 2007), which can cause decreased growth rates, diminished reproduction, and increased post-settlement mortality of juvenile corals (Brooke and Young, 2009). Additionally, the Mauritanian CWCs exist today at temperatures between 9.5 °C and 12 °C (Fig. 7; Ramos et al., 2017), which are close to reported maximum temperatures (~12–14.9 °C) within the distribution range of *L. pertusa* (Davies and Guinotte, 2011; Freiwald et al., 2004; Roberts et al., 2003). Although CWCs can cope to some degree with enhanced temperatures, mound formation seems to stagnate at temperatures above 12 °C (see Wienberg and Titschack, 2017). Moreover, high temperatures also imply elevated respiration rates (Dodds et al., 2007), which further increase the stress on the CWCs on the Mauritanian margin. Consequently, low DOCs in conjunction with relatively high temperatures prevailing today at intermediate depths along the open Mauritanian slope are suggested to represent key factors that hamper an intense coral colonisation, and hence, present-day mound formation.

5.2. Submarine canyons: refuges for cold-water corals and source for coral larvae supply

The present-day higher abundance of live CWCs within the canyons (Fig. 3; Westphal et al., 2012) point to more suitable living conditions for the CWCs there in comparison to the open slope. Submarine canyons are episodically influenced by processes such as cascading of dense shelf waters and turbidity currents that enhance the downslope transport of near surface waters and sediments and associated dissolved and particulate organic matter from the continental shelf to the deep sea (Canals et al., 2006, 2009; Klein et al., 2003; Puig et al., 2008; Pusceddu et al., 2013). The positive feedback of enhanced downslope transport processes within canyons on the proliferation of CWCs has already been suggested for other coral areas (Huvenne et al., 2011; Morris et al., 2013; Orejas et al., 2009; Taviani et al., 2016). One prominent example is the Mediterranean Sea, where living occurrences of *L. pertusa* and *M. oculata* are rather scarce, most likely due to the present-day oligotrophic conditions in combination with relatively high temperatures being close to the known thermal tolerance of these species (Davies and Guinotte, 2011). Nevertheless, various Mediterranean canyons in the Gulf of Lion and in the Adriatic Sea host most vivid coral communities with high quantities of large living colonies of CWCs, which is interpreted to be the consequence of recurring cascading events fuelling the coral ecosystems (Fabri et al., 2014; Orejas et al., 2009; Taviani et al., 2016). In addition, a study assessing the temporal evolution of oxygen concentrations in the Mediterranean Sea indicated a 5-years-interval with considerably elevated oxygen concentrations in deeper waters related to the cascade of oxygen-rich near surface waters into the deep layers (Klein et al., 2003). Hence, it is speculated that the CWCs thriving today within the Mauritanian canyons also benefit from a (potential) regular flushing of the canyons with organic matter-rich and, even more important, with well-oxygenated near surface waters transported downslope that result in more suitable conditions within the canyons compared to the overall oxygen-depleted

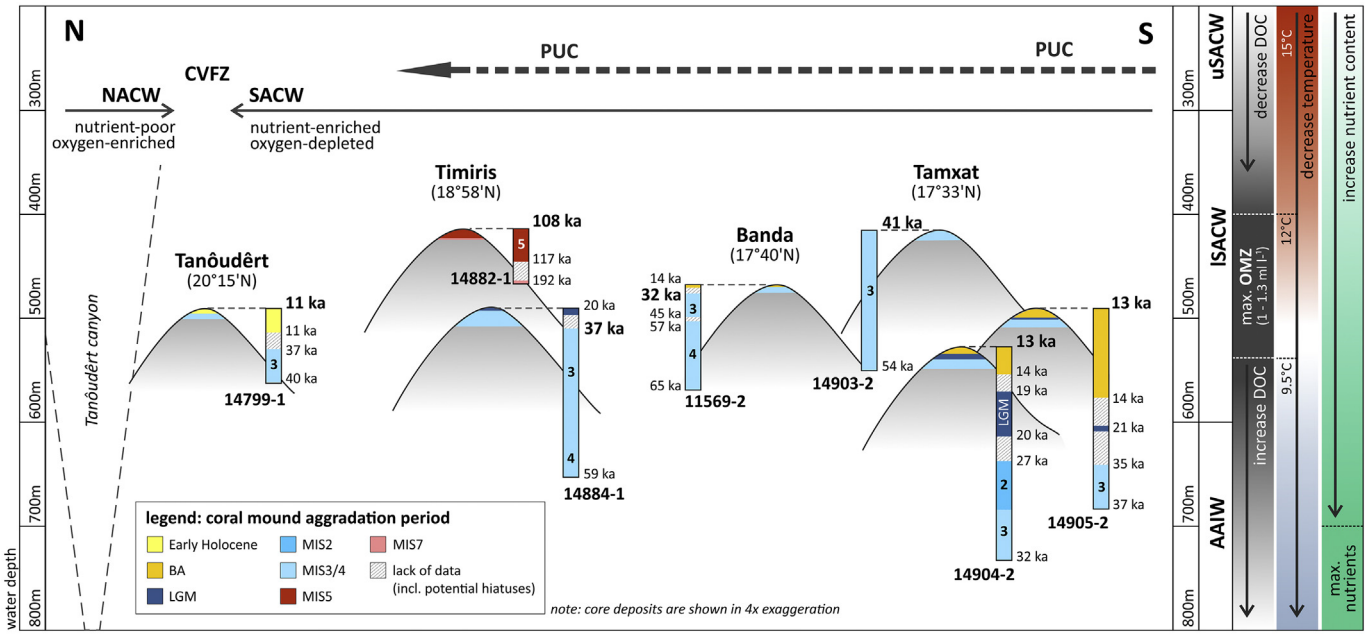

Fig. 7. Schematic north-south cross profile showing the depth position of the studied coral mounds along the Mauritanian margin in relation to the present-day oceanography. The core records (GeoB core ID is placed next to the record) show the mound formation periods (Marine Isotope Stages: MIS 7, 5 to 2; Last Glacial Maximum: LGM; Bølling-Allerød: BA; see legend for colour code) and are displayed in 4× exaggeration next to the respective mound. Timing of the on- and offset of the mound formation periods (numbers given in ka) and the cessation in mound formation (bold numbers) based on the coral ages are provided inside the records. The depth levels of the upper and lower South Atlantic Central Waters (SACW) and the Antarctic Intermediate Water (AAIW) are indicated supplemented by the relative changes of the dissolved oxygen concentration (DOC), water temperature, and nutrient content through depth (compiled after Pastor et al., 2012; Pelegrí et al., 2017; Peña-Izquierdo et al., 2015; Ramos et al., 2017). The extension of the oxygen minimum zone (OMZ) with DOCs of 1.0–1.3 ml l^{-1} is highlighted. The latitudinal extension of the SACW (upper SACW carried by the Poleward Undercurrent: PUC) and the North Atlantic Central Water (NACW), and the position of the Cap Verde frontal zone (CVFZ) are displayed above the mounds. (For interpretation of the references to colour in this figure legend, the reader is referred to the Web version of this article.)

conditions along the open slope.

In addition, as the fossil CWCs collected from the surface of the canyon flanks show ages ranging from 1.1 ka to recent ages (Fig. 5, Table 2), this point to suitable environmental conditions for CWC growth within the canyons already since the Late Holocene. Hence, the question arises whether canyons act as a refuge for the CWCs maintaining their survival. Moreover, canyons might serve as a regional source for larvae supply triggering the documented recent re-colonisation pulse along the open Mauritanian slope (Westphal et al., 2012). A canyon refuge scenario is a likely alternative or an additional re-colonisation pathway to the previously postulated supra-regional larvae migration via climate-driven major recirculation patterns (De Mol et al., 2005; Frank et al., 2011; Henry et al., 2014), and has also already been postulated for submarine canyons along the US east coast (Brooke and Ross, 2014). However, without future molecular genetic studies the source of larvae enabling re-colonisation pulses along the open Mauritanian slope remains speculative.

The herein presented data provide some reliable evidence for a canyon refuge scenario for the last 1.1 kyr, but it lacks direct information about the presence of CWCs in canyons prior to the Late Holocene. The steeply inclined slopes within canyons provoke enhanced post-mortem break-off of coral colonies. Moreover, canyons act as a conduit for turbidity currents (e.g., Hanebuth and Henrich, 2009), which might explain the lack of "older" corals at the upper canyon flanks as the eroding effect of such turbidite events cause a regular downslope export of coral fragments within the canyons.

5.3. Timing, duration and rate of Mauritanian coral mound formation

All core records obtained from the Mauritanian coral mounds (including the record from the Banda mound complex presented by Eisele et al., 2011) clearly display distinct aggradation periods during the last ~120 kyr (Figs. 6 and 7, Table 3). Considering the present-day average mound height of 100 m above the seafloor and the maximum core recovery of 10 m, these cores display the most recent period(s) of mound development. Our records clearly document that mound formation along the Mauritanian margin took place during the MIS5, the last glacial, the BA, and for a very short interval during the very Early Holocene (Figs. 6 and 7).

The associated $AR_{ø}$ vary considerably through time and show an increasing trend from old to young aggradation periods (Table 3). The lowest $AR_{ø}$ of 16 cm kyr^{-1} was obtained for the MIS5 aggradation period of the shallow Timiris mound, which likely displays a period of reduced coral occurrence and/or reduced sediment supply both hampering enhanced mound formation. During the MIS3 all studied mounds (except of the shallow Timiris mound) experienced vertical aggradation with calculated $AR_{ø}$ ranging between 32 and 52 cm kyr^{-1} (Table 3). The highest $AR_{ø}$ of 88–364 cm kyr^{-1} correspond to the most recent aggradation periods since the MIS2 and are restricted to the southern deep Tamxat mounds and the isolated coral mound developed on the southern flank of the Tanôudêrt canyon (Table 3). Maximum ARs of >1000 cm kyr^{-1} were calculated for aggradation periods corresponding to the last deglaciation (mainly BA) and the (very) Early Holocene. In comparison to other coral mound areas in the North Atlantic, these ARs

are in the same range as those described for the Norwegian coral mounds (218–1500 cm kyr^{-1}), which are believed to host the most vivid coral communities discovered so far (López Correa et al., 2012; Titschack et al., 2015). This highlights the exceptional proliferation of the Mauritanian corals during the last glacial until the onset of the Holocene.

The timing of mound development and in particular the timing of the cessation of the latest mound aggradation period varies between the individual mounds. The most striking finding is that coral mound formation in shallower water depths ceased much earlier than in deeper waters (Fig. 7), which clearly points to a temporal displacement of mound formation within the upper and lower mound chains off Mauritania. This is nicely displayed in the two records obtained from the top of a shallow mound (415 m water depth) and a deep mound (490 m water depth) both belonging to the Timiris mound complex (Fig. 2C). The upper part (upper 2 m) of the shallow mound developed during the MIS5 (117 ka - 108 ka). Since then, corals still occasionally occurred on the mound (as revealed by single surface coral ages of 103 ka and 56 ka; Table 2), but mound formation stagnated already for more than 100 kyr and experienced no reactivation since then. In contrast, the record of the deep Timiris mound reveals a much younger aggradation period, that largely coincided with the MIS3 resulting in the deposition of ~8 m of mound sediments within 22 kyr. After ~37 ka, the mound experienced a significant slow-down in mound aggradation, expressed by very low AR of 6 cm kyr^{-1} lasting for ~15 kyr, before mound formation finally stagnated at ~20 ka (Table 3; Fig. 7). CWCs still occasionally colonised this mound at least until the onset of the Holocene at ~11.5 ka as indicated by coral ages obtained from the mound's surface (Fig. 2C; Table 2), but the corals were obviously not capable to maintain mound aggradation. In addition to the reduced occurrence of CWCs, a significant reduction in sediment supply since the termination of the LGM might account for the slow-down and stagnation in mound formation.

For the upper and lower mound chains of the Tamxat mound complex (Fig. 2D), a similar temporal shift in mound aggradation towards deeper depths is identified (Fig. 7). The record for the shallow mound (415 m water depth) reveals a pronounced mound aggradation period during the MIS3, when ~7 m of mound sediments were deposited within ~13 kyr (54 - 41 ka; Table 3), while it experienced no further aggradation since then. The two deep records (>490 m water depth) also reveal mound aggradation during the MIS3. However, in contrast to the shallow mound, they experienced subsequent reactivation of formation during the MIS2 (late LGM) and the BA, which lasted until 13 ka (Figs. 6 and 7).

Interestingly, the isolated coral mound developed on the southern flank of the Tanôudêrt canyon (Fig. 2B) shows a very specific temporal formation pattern. As all other deep coral mounds, it experienced vertical aggradation during the MIS3, followed by an impressive hiatus lasting for about 25 kyr. Only during the very Early Holocene at 11.4 ka, this northernmost coral mound experienced a very intense aggradation period (marked by the deposition of 1 m of mound sediments within 68 years) pointing to a specific environmental setting that allowed an exceptionally, although timely restricted, proliferation of CWCs, which is in complete contrast to the southern coral mounds (Figs. 6 and 7).

5.4. Environmental control on pre-Holocene coral mound formation

During the last glacial, mound formation was active along the entire Mauritanian margin (Fig. 7), which indicates more suitable environmental conditions for sustained CWC growth compared to the present-day situation. Today, the Mauritanian mounds are bathed by the lSACW and occur within the OMZ with very low DOCs and enhanced temperatures (Fig. 7), which is interpreted to be the key control hampering present-day mound formation. The glacial sea level was about 40–100 m lower compared to today (Lambeck and Chappell, 2001), which likely also caused a displacement of the OMZ into deeper waters. If this happened, the Mauritanian mounds were placed above the core of the OMZ towards the uSACW, where higher oxygen concentrations prevail compared to the lSACW (Pastor et al., 2012; Pelegrí et al., 2017; Peña-Izquierdo et al., 2015).

Beside the assumed oxygen control on mound formation, a more vigorous hydrodynamic regime might also account for the glacial success of the Mauritanian coral mounds. Today, the mounds are situated below the PUC, which carries the uSACW northwards between 100 and 300 m depth (Fig. 7) and flows with maximum speeds of ~0.25 m s^{-1} (Pelegrí et al., 2017), while bottom current velocities at the depth level of the mounds are fairly weak with 1–6 cm s^{-1} (Colman et al., 2005 and references therein). However, the development of 20–50 m deep moats east and west of the coral mounds (Fig. 2C–E) point to (at least occasionally) strong and erosive bottom currents in the past (Colman et al., 2005; Ramos et al., 2017). Being influenced by a more energetic setting during the last glacial, mound formation would have benefitted in a twofold way. Strong bottom currents (i) enhance the supply of food particles promoting CWC growth, and (ii) deliver large amounts of suspended sediments, which are entrapped and deposited within the framework, and allow increased vertical mound aggradation (Eisele et al., 2014; Hebbeln et al., 2016; Huvenne et al., 2009; Mienis et al., 2009; Titschack et al., 2015). Thus, the sea level-induced vertical displacement of the Mauritanian coral mounds towards a setting with better ventilated waters and stronger (slope) bottom currents might explain the pronounced glacial mound formation.

Since the LGM, the temporal variation in coral mound formation seems to be the consequence of a lateral shift of distinct oceanographic boundary conditions, which were induced by past displacements of the CVFZ separating the NACW and the SACW. Southward displacements of the CVFZ during the LGM and the BA, allowed the nutrient-poor and well-ventilated NACW to penetrate further to the south (Huang et al., 2012; Romero et al., 2008). This process decreased the ocean surface productivity, but also transported oxygen-enriched waters to the Mauritanian coral mound province south of 20°N. In contrast, during the HE1 and the YD, a northward displacement of the CVFZ increased the northward intrusion of nutrient-rich and oxygen-depleted SACW. This resulted in very high primary production marked by sediments with extremely high biogenic opal concentrations (Huang et al., 2012; Romero et al., 2008). The very high primary production even more caused an increased consumption of oxygen at the seafloor as a result of increased export, deposition and remineralisation of organic matter (Filipsson et al., 2011; Gallego-Torres et al., 2014; McKay et al., 2014). Overall, changes in the palaeo-productivity are certainly no key control on mound formation along the Mauritanian margin as primary production was always relatively high even though it varied on millennial timescales (and also across glacial-interglacial cycles; Matsuzaki et al., 2011; Romero et al., 2008). Moreover, during rather moderate productivity conditions prevailing during the BA, CWCs experienced their most prolific period expressed by very high mound ARs (Fig. 6, Table 3), while during the most productive period corresponding to the HE1, mound formation temporarily stagnated. In contrast, past variations in DOCs caused by the latitudinal shifts of the CVFZ that regulated the northward intrusion of the oxygen-depleted SACW, fit well to the mound formation pattern observed since the LGM. Thus, despite the overall productive conditions, extremely low DOCs prevailing during the HE1 and YD prevented a widespread occurrence of CWC and caused a stagnation or slow-down in

mound formation.

The retreat of the CWCs from the coral mounds along the entire slope since the early Holocene is attributed to the consequence of the drastic environmental changes induced by the rapid deglacial sea level rise since ~16.5 ka (Hanebuth et al., 2000; Lambeck et al., 2014). The deglacial sea level rise caused a fast drowning of the Mauritanian shelf, a landward displacement of the coastline (for the broad northern shelf over a distance of ~100 km), and consequently a drastic displacement of depocenters from the slope to the shelf (Hanebuth and Lantzsch, 2008), which in turn implied a reduced seaward advection of particulate organic material (Bertrand et al., 2000). Thus, the processes induced by the rapid sea level rise likely had severe consequences for the CWCs and the coral mounds sitting on the upper to middle slope as it reduced the availability of food triggering coral growth and it decreased the supply of sediments being essential for mound aggradation. Finally, at ~8 ka sea level reached a position just a few metres below its modern level (Hanebuth et al., 2000; Lambeck et al., 2014), that probably placed the Mauritanian coral mounds already at this time right to an oxygen-deficient environment.

5.5. Cessation of Mauritanian coral mound formation and the lack of subsequent deposits

A key finding of the present study is that coral mound formation along the entire Mauritanian margin ultimately ceased with the onset of the Holocene and experienced no reactivation until today although scarce CWC growth is documented. Cessation in mound formation occurred already at ~108 ka and ~41 ka, respectively, for the shallow mounds of the Timiris and Tamxat mound complexes, while their deeper counterparts were active until ~37 ka and ~13 ka, respectively, and aggradation on the deep mound of the Tanôudêrt canyon lasted until ~11 ka (Fig. 7). It is remarkable that all Mauritanian coral mounds experienced no significant coverage or burial by sediments since their most recent aggradation period. Until today, the fossil corals on the mounds' surface remained largely exposed being subject to strong bioerosion due to the lack of a sediment cover. This pattern has already been documented for other coral mound areas, such as the Moroccan margin, where mounds covered by fossil corals are still exposed though mound formation ceased at ~10 ka (Wienberg et al., 2010, 2009). It has also been identified in the fossil record as numerous sediment cores collected from coral mounds show partly extended hiatuses covering several thousands of years (e.g., Dorschel et al., 2005; Eisele et al., 2008; Frank et al., 2009; López Correa et al., 2012; Matos et al., 2017; this study) or even ~800 kyr as observed for the prominent IODP record drilled from Challenger mound along the Irish margin (Kano et al., 2007). Such hiatuses indicate that the mounds experienced no significant burial when they were not covered by living CWCs, while concurrently deposition took place in the surrounding area (e.g., Titschack et al., 2009).

On the Mauritanian coral mounds, the following scenarios might explain the lack of deposits since they are in a dormant stage. The rapid deglacial sea level rise caused a landward displacement of the coastline shifting the depocenter of particulate organic material towards the shelf (Hanebuth and Lantzsch, 2008), while seaward advection of suspended sediment decreased, both resulting in low slope sedimentation (Bertrand et al., 2000). Low sedimentation rates of ~10 cm kyr^{-1} are reported for the Holocene (e.g. Romero et al., 2008). However, even such low sedimentation rates would result in the deposition of 1–10 m of sediments on top of the mounds when considering the range of exposure time of the Mauritanian coral mounds. In addition, sub-sedimentary formed coral limestone blocks were detected exposed on top of some mounds belonging to the Banda and Tamxat mound complexes (Westphal et al., 2012). This argues for frequently occurring highly dynamic events that flush over the mounds' tops and are energetic enough to efficiently remove formerly deposited sediments. Potential candidates triggering such processes are storm events or tsunami waves, the latter generated by the numerous landslide events that occurred in the area (see Fig. 2A; De Mol et al., 2009; Urlaub et al., 2015). For example, the Tamxat mounds, which are located just upslope of the headwall scarp of the Mauritania slide complex, are rooted on a lower reflector than the slide plane, and thus are older than the slope failure (De Mol et al., 2009), and must have experienced several slide events. Another suspect explaining the exposed nature of the Mauritanian mounds is the intense along-slope PUC. This slope current was identified from Guinea up to Iberia (Pelegrí et al., 2017), and its erosive effect probably formed the up to 50 m deep moats developed at the foot of the Mauritanian coral mounds (Fig. 2C–E; Colman et al., 2005). Such slope currents would prevent the sustained deposition of fine sediments on top of the mounds by winnowing (selective erosion at flow speeds >10–15 cm s^{-1}; McCave et al., 2017). During active phases when the mounds are covered by living CWCs, sedimentation of fine sediments is enhanced due to the baffling capacity of the open coral framework even though strong currents prevail (Huvenne et al., 2009; Titschack et al., 2009).

6. Conclusions

The Mauritanian coral mound province in the Atlantic Ocean is outstanding because of its giant dimension (400 km long, 100 m high) and its special morphological configuration of two almost continuous slope-parallel mound chains (Fig. 2). Located underneath the NW African eastern boundary upwelling system, the Mauritanian coral mound province occurs in one of the most productive areas in the marine realm.

The herein presented new coral age dataset documents that the coral mounds along the entire Mauritanian margin are in a dormant state since the onset of the Holocene. The pre-Holocene mound development was not uniform and shows a complex spatiotemporal pattern as timing and AR of distinct aggradation periods differed between the studied mounds in relation to their position on the slope (latitude and water depth; Figs. 6 and 7). During the last glacial, pronounced CWC growth favoured enhanced coral mound formation ($AR_{ø}$: 32–192 cm kyr^{-1}) along the entire Mauritanian margin and at all depths (except of the shallow Timiris mound). Most prolific periods with remarkably high vertical mound ARs of up to 1600 cm kyr^{-1} occurred during the BA and the (very) Early Holocene and were restricted to the isolated Tanôudêrt canyon mound in the north and the deep Tamxat mounds in the south. Striking is the observation that mound formation was also active during the Last Interglacial (MIS5), though restricted to the shallow Timiris mounds (415 m water depth) with a low $AR_{ø}$ of 16 cm kyr^{-1}.

The observed spatiotemporal pattern in mound formation suggests a strong link to changes in the water column structure and central water mass circulation. Today, the mounds are exposed to very low DOCs (1.0–1.3 ml l^{-1}; Ramos et al., 2017), which are the combined result of an increased oxygen consumption by intense organic matter remineralisation and the lateral supply of oxygen-depleted SACW from the south. The low oxygen conditions in conjunction with enhanced water temperatures (9.5–12 °C; Ramos et al., 2017) are suggested as the main stressors that determine the present-day scarce occurrence of live CWCs, and thus, the dormant state of the mounds. In the past, vertical and lateral shifts of the oxygen-depleted southern-sourced SACW were triggered by sea level variations and/or displacements of the CVFZ. Consequently, the coral mounds were placed towards or out of oxygen-depleted

waters, which would largely explain the observed mound formation pattern. Overall, this study suggests oxygen in combination with temperature as key factors controlling mound formation along the Mauritanian margin. Better ventilated conditions and potentially lower temperatures promoted CWC growth, and thus, vertical mound aggradation during the last glacial, the late LGM and the BA, while low-oxygenated (and warmer) conditions during the HE1, the (late) YD and during the Holocene caused a slow-down or stagnation in mound formation. However, low bottom water oxygenation alone cannot explain the entire observed formation pattern. The persistent dormant state of the shallow Timiris mound since the MIS5 clearly suggests further environmental factors (such as bottom current strength, sediment supply, temperature) stimulating or suppressing mound formation. However, to unravel the entire set and complex interplay of environmental and oceanographic controls on coral mound formation along the Mauritanian margin, further studies concentrating on intermediate water mass reconstruction (including water mass properties) are needed.

The numerous canyons along the Mauritanian margin provide an additional habitat for CWCs. There, CWCs occur frequently since the Late Holocene until today, while live CWCs are only rarely documented from the coral mounds. This is ascribed to the special oceanographic conditions related to canyons. Regular downslope transport of oxygen-enriched surface waters and particulate organic material may bring about better environmental boundary conditions to sustain CWC growth, and thus, refuges at times of overall stressful environmental conditions along the open continental slope. Canyons might, therefore, act as a larvae source to restore the CWC re-colonisation of the mounds along the slope.

Acknowledgements

We like to thank the nautical and scientific crews, in particular chief scientist H. Westphal and the geo-lab team T. Hanebuth, H. Lantzsch and B. Kockisch, for on-board assistance during R/V MARIA S. MERIAN cruise MSM16-3. The research leading to these results has received support from the *Deutsche Forschungsgemeinschaft* (DFG) through providing ship time. The cruise was further supported through the DFG Research Center/Cluster of Excellence "MARUM – The Ocean in the Earth System". We kindly acknowledge R. Eichstädter and F. Thil for lab support during the Uranium-series dating. For taxonomical identification, we thank M. Türkay (decapods) and I. Sampaio (octocorals). We further thank the GeoB Core Repository at the MARUM for the assistance in providing sediment cores and sample material. We dearly acknowledge V. Huvenne and G. Eberli for their comments that have greatly improved the manuscript. This study received funding from and contributes to the DFG-projects "Palaeo-WACOM" (HE 3412/17-1) and "Cold-water coral mound development in a tropical upwelling cell – the great wall of(f) Mauritania" (Ti 706/3-1). A. Freiwald received funding from the Hessian initiative for the development of scientific and economic excellence (LOEWE) at the Biodiversity and Climate Research Centre (BiK-F), Frankfurt, Germany. This is ISMAR-CNR Bologna scientific contribution n.1932. The data reported in this paper are archived in Pangaea (www.pangaea.de).

Appendix A. Supplementary data

Supplementary data related to this article can be found at https://doi.org/10.1016/j.quascirev.2018.02.012.

References

Andersen, M.B., Stirling, C.H., Zimmermann, B., Halliday, A.N., 2010. Precise determination of the open ocean $^{234}U/^{238}U$ composition. G-cubed 11, Q12003.
Antobreh, A.A., Krastel, S., 2006. Morphology, seismic characteristics and development of Cap Timiris Canyon, offshore Mauritania: a newly discovered canyon preserved off a major arid climatic region. Mar. Petrol. Geol. 23, 37–59.
Antobreh, A.A., Krastel, S., 2007. Mauritania Slide Complex: morphology, seismic characterisation and processes of formation. Int. J. Earth Sci. 96, 451–472.
Arístegui, J., Barton, E.D., Álvarez-Salgado, X.A., Santos, A.M.P., Figueiras, F.G., Kifani, S., Hernández-León, S., Mason, E., Machú, E., Demarcq, H., 2009. Sub-regional ecosystem variability in the Canary Current upwelling. Prog. Oceanogr. 83, 33–48.
Barton, E.D., 1989. The poleward undercurrent on the eastern boundary of the Subtropical North Atlantic. In: Neshyba, S., Smith, R.L., Mooers, C.N.K. (Eds.), Poleward Flows along Eastern Ocean Boundaries. Springer, Lecture Note Series, pp. 82–95.
Behrenfeld, M.J., Falkowski, P.G., 1997. Photosynthetic rates derived from satellite-based chlorophyll concentration. Limnol. Oceanogr. 42, 1–20.
Bertrand, P., Pedersen, T.F., Martinez, P., Calvert, S., Shimmield, G., 2000. Sea level impact on nutrient cycling in coastal upwelling areas during deglaciation: evidence from nitrogen isotopes. Global Biogeochem. Cycles 14, 341–355.
Brooke, S., Ross, S.W., 2014. First observations of the cold-water coral *Lophelia pertusa* in mid-Atlantic canyons of the USA. Deep Sea Res. Part II 104, 245–251.
Brooke, S., Young, C.M., 2009. In situ measurement of survival and growth of *Lophelia pertusa* in the northern Gulf of Mexico. Mar. Ecol. Prog. Ser. 397, 153–161.
Büscher, J.V., Form, A.U., Riebesell, U., 2017. Interactive effects of ocean acidification and warming on growth, fitness and survival of the cold-water coral *Lophelia pertusa* under different food availabilities. Fron. Mar. Sci. 4, 101.
Canals, M., Danovaro, R., Heussner, S., Lykousis, V., Puig, P., Trincardi, F., Calafat, A.M., Durrieu de Madron, X., Palanques, A., Sànchez-Vidal, A., 2009. Cascades in Mediterranean submarine grand canyons. Oceanography 22, 26–43.
Canals, M., Puig, P., Durrieu de Madron, X., Heussner, S., Palanques, A., Fabrés, J., 2006. Flushing submarine canyons. Nature 444, 354–357.
Carr, M.-E., Kearns, E.J., 2003. Production regimes in four eastern boundary current systems. Deep-Sea Res. Part II 50, 3199–3221.
Cheng, H., Adkins, J., Edwards, R.L., Boyle, E.A., 2000. U-Th dating of deep-sea corals. Geochem. Cosmochim. Acta 64, 2401–2416.
Colman, J.G., Gordon, D.M., Lane, A.P., Forde, M.J., Fitzpatrick, J., 2005. Carbonate mounds off Mauritania, Northwest Africa: status of deep-water corals and implications for management of fishing and oil exploration activities. In: Freiwald, A., Roberts, J.M. (Eds.), Cold-water Corals and Ecosystems. Springer, Heidelberg, pp. 417–441.
Davies, A.J., Duineveld, G.C.A., Lavaleye, M.S.S., Bergman, M.J., van Haren, H., Roberts, J.M., 2009. Downwelling and deep-water bottom currents as food supply mechanisms to the cold-water coral *Lophelia pertusa* (Scleractinia) at the Mingulay Reef Complex. Limnol. Oceanogr. 54, 620–629.
Davies, A.J., Duineveld, G.C.A., van Weering, T.C.E., Mienis, F., Quattrini, A.M., Seim, H.E., Bane, J.M., Ross, S.W., 2010. Short-term environmental variability in cold-water coral habitat at Viosca Knoll, Gulf of Mexico. Deep-Sea Res. Part I 57, 199–212.
Davies, A.J., Guinotte, J.M., 2011. Global habitat suitability for framework-forming cold-water corals. PLoS One 6, e18483.
De Mol, B., Henriet, J.-P., Canals, M., 2005. Development of coral banks in the Porcupine Seabight: do they have Mediterranean ancestors? In: Freiwald, A., Roberts, J.M. (Eds.), Cold-water Corals and Ecosystems. Springer, Heidelberg, pp. 515–533.
De Mol, B., Huvenne, V.A.I., Canals, M., 2009. Cold-water coral banks and submarine landslides: a review. Int. J. Earth Sci. 98, 885–899.
Dodds, L.A., Roberts, J.M., Taylor, A.C., Marubini, F., 2007. Metabolic tolerance of the cold-water coral *Lophelia pertusa* (Scleractinia) to temperature and dissolved oxygen change. J. Exp. Mar. Biol. Ecol. 349, 205–214.
Dorschel, B., Hebbeln, D., Rüggeberg, A., Dullo, W.-C., 2005. Growth and erosion of a cold-water coral covered carbonate mound in the Northeast Atlantic during the Late Pleistocene and Holocene. Earth Planet Sci. Lett. 233, 33–44.
Douarin, M., Elliot, M., Noble, S.R., Sinclair, D., Henry, L.-A., Long, D., Moreton, S.G., Murray Roberts, J., 2013. Growth of north-east Atlantic cold-water coral reefs and mounds during the Holocene: a high resolution U-series and ^{14}C chronology. Earth Planet Sci. Lett. 375, 176–187.
Douville, E., Sallé, E., Frank, N., Eisele, M., Pons-Branchu, E., Ayrault, S., 2010. Rapid and accurate Th-U dating on ancient carbonates using inductivity coupled plasma-quadrupole mass spectrometry. Chem. Geol. 272, 1–11.
Duineveld, G.C.A., Jeffreys, R.M., Lavaleye, M.S.S., Davies, A.J., Bergman, M.J.N., Watmough, T., Witbaard, R., 2012. Spatial and tidal variation in food supply to shallow cold-water coral reefs of the Mingulay Reef complex (Outer Hebrides, Scotland). Mar. Ecol. Prog. Ser. 444, 97–115.
Eisele, M., Frank, N., Wienberg, C., Hebbeln, D., López Correa, M., Douville, E., Freiwald, A., 2011. Productivity controlled cold-water coral growth periods during the last glacial off Mauritania. Mar. Geol. 280, 143–149.
Eisele, M., Frank, N., Wienberg, C., Titschack, J., Mienis, F., Beuck, L., Tisnerat-Laborde, N., Hebbeln, D., 2014. Sedimentation patterns on a cold-water coral mound off Mauritania. Deep-Sea Res. Part II 99, 307–315.
Eisele, M., Hebbeln, D., Wienberg, C., 2008. Growth history of a cold-water coral covered carbonate mound - galway Mound, Porcupine Seabight, NE-Atlantic. Mar. Geol. 253, 160–169.
Fabri, M.C., Pedel, L., Beuck, L., Galgani, F., Hebbeln, D., Freiwald, A., 2014. Megafauna

of vulnerable marine ecosystems in French Mediterranean submarine canyons: spatial distribution and anthropogenic impacts. Deep-Sea Res. Part II 104, 184–207.
Filipsson, H.L., Romero, O.E., Stuut, J.-B.W., Donner, B., 2011. Relationships between primary productivity and bottom-water oxygenation off northwest Africa during the last deglaciation. J. Quat. Sci. 26, 448–456.
Fink, H.G., Wienberg, C., De Pol-Holz, R., Hebbeln, D., 2015. Spatio-temporal distribution patterns of Mediterranean cold-water corals (*Lophelia pertusa* and *Madrepora oculata*) during the past 14,000 years. Deep-Sea Res. Part I 103, 37–48.
Fink, H.G., Wienberg, C., Hebbeln, D., McGregor, H.V., Schmiedl, G., Taviani, M., Freiwald, A., 2012. Oxygen control on Holocene cold-water coral development in the eastern Mediterranean Sea. Deep-Sea Res. Part I 62, 89–96.
Fischer, G., Reuter, C., Karakas, G., Nowald, N., Wefer, G., 2009. Offshore advection of particles within the Cape Blanc filament, Mauritania: results from observational and modelling studies. Prog. Oceanogr. 83, 322–330.
Flögel, S., Dullo, W.C., Pfannkuche, O., Kiriakoulakis, K., Rüggeberg, A., 2014. Geochemical and physical constraints for the occurrence of living cold-water corals. Deep-Sea Res. Part II 99, 19–26.
Fosså, J.H., Lindberg, B., Christensen, O., Lundälv, T., Svellingen, I., Mortensen, P.B., Alsvag, J., 2005. Mapping of *Lophelia* reefs in Norway: experiences and survey methods. In: Freiwald, A., Roberts, J.M. (Eds.), Cold-water Corals and Ecosystems. Springer, Heidelberg, pp. 359–391.
Frank, N., Freiwald, A., López Correa, M., Wienberg, C., Eisele, M., Hebbeln, D., Van Rooij, D., Henriet, J.-P., Colin, C., van Weering, T.C.E., de Haas, H., Buhl-Mortensen, P., Roberts, J.M., De Mol, B., Douville, E., Blamart, D., Hatte, C., 2011. Northeastern Atlantic cold-water coral reefs and climate. Geology 39, 743–746.
Frank, N., Paterne, M., Ayliffe, L., van Weering, T.C.E., Henriet, J.-P., Blamart, D., 2004. Eastern North Atlantic deep-sea corals: tracing upper intermediate water $\Delta^{14}C$ during the Holocene. Earth Planet Sci. Lett. 219, 297–309.
Frank, N., Ricard, E., Lutringer-Paquet, A., van der Land, C., Colin, C., Blamart, D., Foubert, A., Van Rooij, D., Henriet, J.-P., de Haas, H., van Weering, T.C.E., 2009. The Holocene occurrence of cold water corals in the NE Atlantic: implications for coral carbonate mound evolution. Mar. Geol. 266, 129–142.
Freiwald, A., Fosså, J.H., Grehan, A., Koslow, T., Roberts, J.M., 2004. Cold-water Coral Reefs. UNEP-WCMC, Cambridge, UK. Biodiversity Series 22.
Gallego-Torres, D., Romero, O.E., Martínez-Ruiz, F., Kim, J.-H., Donner, B., Ortega-Huertas, M., 2014. Rapid bottom-water circulation changes during the last glacial cycle in the coastal low-latitude NE Atlantic. Quat. Res. 81, 330–338.
Glogowski, S., Dullo, W.C., Feldens, P., Liebetrau, V., von Reumont, J., Hühnerbach, V., Krastel, S., Wynn, R.B., Flögel, S., 2015. The Eugen Seibold coral mounds offshore western Morocco: oceanographic and bathymetric boundary conditions of a newly discovered cold-water coral province. Geo Mar. Lett. 35, 257–269.
Grasmueck, M., Eberli, G.P., Viggiano, D.A., Correa, T., Rathwell, G., Luo, J., 2006. Autonomous underwater vehicle (AUV) mapping reveals coral mound distribution, morphology, and oceanography in deep water of the Straits of Florida. Geophys. Res. Lett. 33, L23616,. https://doi.org/10.1029/2006GL027734.
Guinotte, J.M., Orr, J., Cairns, S., Freiwald, A., Morgan, L., George, R., 2006. Will human-induced changes in seawater chemistry alter the distribution of deep-sea scleractinian corals? Front. Ecol. Environ. 4, 141–146.
Hanebuth, T.J.J., Stattegger, K., Grootes, P.M., 2000. Rapid flooding of the Sunda Shelf - a late-glacial sea-level record. Science 288, 1033–1035.
Hanebuth, T.J.J., Henrich, R., 2009. Recurrent decadal-scale dust events over Holocene western Africa and their control on canyon turbidite activity (Mauritania). Quat. Sci. Rev. 28, 261–270.
Hanebuth, T.J.J., Lantzsch, H., 2008. A Late Quaternary sedimentary shelf system under hyperarid conditions: unravelling climatic, oceanographic and sea-level controls (Golfe d'Arguin, Mauritania, NW Africa). Mar. Geol. 256, 77–89.
Harrison, S.P., Kohfeld, K.E., Roelandt, C., Claquin, T., 2001. The role of dust in climate changes today, at the Last Glacial Maximum and in the future. Earth Sci. Rev. 54, 43–80.
Hebbeln, D., Samankassou, E., 2015. Where did ancient carbonate mounds grow - in bathyal depths or in shallow shelf waters? Earth Sci. Rev. 145, 56–65.
Hebbeln, D., Van Rooij, D., Wienberg, C., 2016. Good neighbours shaped by vigorous currents: cold-water coral mounds and contourites in the North Atlantic. Mar. Geol. 378, 171–185.
Hebbeln, D., Wienberg, C., Wintersteller, P., Freiwald, A., Becker, M., Beuck, L., Dullo, C., Eberli, G.P., Glogowski, S., Matos, L., Forster, N., Reyes-Bonilla, H., Taviani, M., 2014. Environmental forcing of the Campeche cold-water coral province, southern Gulf of Mexico. Biogeosciences 11, 1799–1815.
Henrich, R., Cherubini, Y., Meggers, H., 2010. Climate and sea level induced turbidite activity in a canyon system offshore the hyperarid Western Sahara (Mauritania): the Timiris Canyon. Mar. Geol. 275, 178–198.
Henrich, R., Hanebuth, T.J.J., Krastel, S., Neubert, N., Wynn, R.B., 2008. Architecture and sediment dynamics of the Mauritania slide complex. Mar. Petrol. Geol. 25.
Henry, L.-A., Frank, N., Hebbeln, D., Wienberg, C., Robinson, L., van de Flierdt, T., Dahl, M., Douarin, M., Morrison, C.L., López Correa, M., Rogers, A.D., Ruckelshausen, M., Roberts, J.M., 2014. Global ocean conveyor lowers extinction risk in the deep sea. Deep-Sea Res. Part I 88, 8–16.
Huang, E., Mulitza, S., Paul, A., Groeneveld, J., Steinke, S., Schulz, M., 2012. Response of eastern tropical Atlantic central waters to Atlantic meridional overturning circulation changes during the Last Glacial Maximum and Heinrich Stadial 1. Paleoceanography 27, PA3229.
Huvenne, V.A.I., Tyler, P.A., Masson, D.G., Fisher, E.H., Hauton, C., Hühnerbach, V., Le Bas, T.P., Wolff, G.A., 2011. A picture on the wall: innovative mapping reveals cold-water coral refuge in submarine canyon. PLoS One 6 (12), e28755.
Huvenne, V.A.I., Van Rooij, D., De Mol, B., Thierens, M., O'Donnell, R., Foubert, A., 2009. Sediment dynamics and palaeo-environmental context at key stages in the Challenger cold-water coral mound formation: clues from sediment deposits at the mound base. Deep-Sea Res. Part I 56, 2263–2280.
Jakobi, R.D., Hayes, D.E., 1982. Bathymetry, microphysiography and reflectivity characteristics of the West African margin between Sierra Leone and Mauritania. In: Von Rad, U., Hinz, K., Sarnthein, M., Seibold, E. (Eds.), Geology of the Northwest African Continental Margin. Springer, Berlin-Heidelberg, pp. 182–210.
Kano, A., Ferdelman, T.G., Williams, T., Henriet, J.-P., Ishikawa, T., Kawagoe, N., Takashima, C., Kakizaki, Y., Abe, K., Sakai, S., Browning, E.L., Li, X., Integrated Ocean Drilling Program Expedition 307 Scientists, 2007. Age constraints on the origin and growth history of a deep-water coral mound in the northeast Atlantic drilled during Integrated Ocean Drilling Program Expedition 307. Geology 35, 1051–1054.
Karakas, G., Nowald, N., Blaas, M., Marchesiello, P., Frickenhaus, S., Schlitzer, R., 2006. High-resolution modeling of sediment erosion and particle transport across the northwest African shelf. J. Geophys. Res. 111, C06025.
Karstensen, J., Stramma, L., Visbeck, M., 2008. Oxygen minimum zones in the eastern tropical Atlantic and Pacific oceans. Prog. Oceanogr. 77, 331–350.
Klein, B., Roether, W., Kress, N., Manca, B.B., Ribera d'Alcala, M., Souvermezoglou, E., Theocharis, A., Civitarese, G., Luchetta, A., 2003. Accelerated oxygen consumption in eastern Mediterranean deep waters following the recent changes in thermohaline circulation. J. Geophys. Res.: Oceans 108 (C9), 8107.
Lambeck, K., Chappell, J., 2001. Sea level change through the last glacial cycle. Science 292, 679–686.
Lambeck, K., Rouby, H., Purcell, A., Sun, Y., Sambridge, M., 2014. sea level and global ice volumes from the last glacial maximum to the Holocene. Proc. Natl. Acad. Sci. Unit. States Am. 111, 15296–15303.
Lindberg, B., Mienert, J., 2005. Postglacial carbonate production by cold-water corals on the Norwegian Shelf and their role in the global carbonate budget. Geology 33, 537–540.
Lisiecki, L., Raymo, M., 2005. A Pliocene-Pleistocene stack of 57 globally distributed benthic δ18O records. Paleoceanography 20, PA1003,. https://doi.org/10.1029/2004PA001071.
López Correa, M., Montagna, P., Joseph, N., Rüggeberg, A., Fietzke, J., Flögel, S., Dorschel, B., Goldstein, S.L., Wheeler, A.J., Freiwald, A., 2012. Preboreal onset of cold-water coral growth beyond the Arctic Circle revealed by coupled radiocarbon and U-series dating and neodymium isotopes. Quat. Sci. Rev. 34, 24–43.
Matos, L., Mienis, F., Wienberg, C., Frank, N., Kwiatkowski, C., Groeneveld, J., Thil, F., Abrantes, F., Cunha, M.R., Hebbeln, D., 2015. Interglacial occurrence of cold-water corals off Cape Lookout (NW atlantic): first evidence of the Gulf stream influence. Deep-Sea Res. Part I 105, 158–170.
Matos, L., Wienberg, C., Titschack, J., Schmiedl, G., Frank, N., Abrantes, F., Cunha, M.R., Hebbeln, D., 2017. Coral mound development at the Campeche cold-water coral province, southern Gulf of Mexico: implications of Antarctic Intermediate Water increased influence during interglacials. Mar. Geol. 392, 53–65.
Matsuzaki, K.M.R., Eynaud, F., Malaizé, B., Grousset, F.E., Tisserand, A., Rossignol, L., Charlier, K., Jullien, E., 2011. Paleoceanography of the Mauritanian margin during the last two climatic cycles: from planktonic foraminifera to African climate dynamics. Mar. Micropaleontol. 79, 67–79.
McCave, I.N., Thornalley, D.J.R., Hall, I.R., 2017. Relation of sortable silt grain-size to deep-sea current speeds: calibration of the 'Mud Current Meter'. Deep-Sea Res. Part I 127, 1–12.
McKay, C.L., Filipsson, H.L., Romero, O.E., Stuut, J.B.W., Donner, B., 2014. Pelagic–benthic coupling within an upwelling system of the subtropical northeast Atlantic over the last 35 ka BP. Quat. Sci. Rev. 106, 299–315.
Mienis, F., de Stigter, H.C., de Haas, H., van Weering, T.C.E., 2009. Near-bed particle deposition and resuspension in a cold-water coral mound area at the Southwest Rockall Trough margin, NE Atlantic. Deep Sea Res. I 56, 1026–1038.
Mienis, F., de Stigter, H.C., White, M., Duineveld, G.C.A., de Haas, H., van Weering, T.C.E., 2007. Hydrodynamic controls on cold-water coral growth and carbonate-mound development at the SW and SE Rockall Trough Margin, NE Atlantic Ocean. Deep-Sea Res. Part I 54, 1655–1674.
Minas, H.J., Packard, T.T., Minas, M., Coste, B., 1982. An analysis of the production-regeneration system in the coastal upwelling area off N.W. Africa based on oxygen, nitrate and ammonium distributions. J. Mar. Res. 40, 615–641.
Mittelstaedt, E., 1983. The upwelling area off northwest Africa - a description of phenomena related to coastal upwelling. Prog. Oceanogr. 12, 307–331.
Mittelstaedt, E., 1991. The ocean boundary along the northwest African coast: circulation and oceanographic properties at the sea surface. Prog. Oceanogr. 26, 307–355.
Morris, K.J., Tyler, P.A., Masson, D.G., Huvenne, V.I.A., Rogers, A.D., 2013. Distribution of cold-water corals in the Whittard canyon, NE Atlantic Ocean. Deep-Sea Res. Part II 92, 136–144.
Nykjær, L., Van Camp, L., 1994. Seasonal and interannual variability of coastal upwelling along northwest Africa and Portugal from 1981 to 1991. J. Geophys. Res. 99, 14197–14207.
Orejas, C., Gori, A., Lo Iacono, C., Puig, P., Gili, J.M., Dale, M.R., 2009. Cold-water corals in the Cap de Creus canyon (north-western Mediterranean): spatial distribution, density and anthropogenic impact. Mar. Ecol. Prog. Ser. 397, 37–51.
Orr, J.C., Fabry, V.J., Aumont, O., Bopp, L., Doney, S.C., Feely, R.A., Gnanadesikan, A., Gruber, N., Ishida, A., Joos, F., Key, R.M., Lindsay, K., Maier-Reimer, E., Matear, R.,

Monfray, P., Mouchet, A., Najjar, R.G., Plattner, G.-K., Rodgers, K.B., Sabine, C.L., Sarmiento, J.L., Schlitzer, R., Slater, R.D., Totterdell, I.J., Weirig, M.-F., Yamanaka, Y., Yool, A., 2005. Anthropogenic ocean acidification over the twenty-first century and its impact on calcifying organisms. Nature 437, 681–686.

Pastor, M.V., Pelegrí, J.L., Hernandez-Guerra, A., Font, J., Salat, J., Emelianov, M., 2008. Water and nutrient fluxes off northwest Africa. Continent. Shelf Res. 28, 915–936.

Pastor, M.V., Peña-Izquierdo, J., Pelegrí, J.L., Marrero-Díaz, Á., 2012. Meridional changes in water mass distributions off NW Africa during November 2007/2008. Cienc. Mar. 38, 223–244.

Paull, C.K., Neumann, A.C., am Ende, B.A., Ussler III, W., Rodriguez, N.M., 2010. Lithoherms on the Florida–Hatteras slope. Mar. Geol. 166, 83–101.

Pelegrí, J.L., Peña-Izquierdo, J., Machín, F., Meiners, C., Presas-Navarro, C., 2017. Oceanography of the Cape Verde basin and Mauritanian slope waters. In: Ramos, A., Ramil, F., Sanz, J.L. (Eds.), Deep-sea Ecosystems off Mauritania: Research of Marine Biodiversity and Habitats in the Northwest African Margin. Springer Netherlands, Dordrecht, pp. 119–153.

Peña-Izquierdo, J., van Sebille, E., Pelegrí, J.L., Sprintall, J., Mason, E., Llanillo, P.J., Machín, F., 2015. Water mass pathways to the North Atlantic oxygen minimum zone. J. Geophys. Res.: Oceans 120, 3350–3372.

Peña→Izquierdo, J., Pelegrí, J.L., Pastor, M.V., Castellanos, P., Emelianov, M., Gasser, M., Salvador, J., Vázquez→Domínguez, E., 2012. The continental slope current system between Cape Verde and the Canary Islands. Sci. Mar. 76, 65–78.

Puig, P., Palanques, A., Orange, D.L., Lastras, G., Canals, M., 2008. Dense shelf water cascades and sedimentary furrow formation in the Cap de Creus Canyon, northwestern Mediterranean Sea. Continent. Shelf Res. 28, 2017–2030.

Pusceddu, A., Mea, M., Canals, M., Heussner, S., Durrieu de Madron, X., Sanchez-Vidal, A., Bianchelli, S., Corinaldesi, C., Dell'Anno, A., Thomsen, L., Danovaro, R., 2013. Major consequences of an intense dense shelf water cascading event on deep-sea benthic trophic conditions and meiofaunal biodiversity. Biogeosciences 10, 2659–2670.

Raddatz, J., Rüggeberg, A., Liebetrau, V., Foubert, A., Hathorne, E.C., Fietzke, J., Eisenhauer, A., Dullo, W.-C., 2014. Environmental boundary conditions of cold-water coral mound growth over the last 3 million years in the Porcupine Seabight, Northeast Atlantic. Deep-Sea Res. Part II 99, 227–236.

Ramos, A., Alcalá, C., Fernández, F., Fernández, L., González-Porto, M., López, V., Moya, J.A., Pascual, P., Presas, C., Puerto, M.A., Ramil, F., Salmerón, F., Sanz, J.L., Rey, J., Viscasillas, L., Abed, J.O., Baye, S.O., Ciré, B.A., Mohamed, B.O., Samba, A.O., Valy, Y.O., 2010. Estudio de los ecosistemas de la plataforma y margen continental de Mauritania. Informe de resultados de la campaña 'Maurit-0911'. Inf Técn IEO-IMROP, p. 161.

Ramos, A., Sanz, J.L., Ramil, F., Agudo, L.M., Presas-Navarro, C., 2017. The giant cold-water coral mounds barrier off Mauritania. In: Ramos, A., Ramil, F., Sanz, J.L. (Eds.), Deep-sea Ecosystems off Mauritania: Research of Marine Biodiversity and Habitats in the Northwest African Margin. Springer Netherlands, Dordrecht, pp. 481–525.

Roberts, J.M., Long, D., Mortensen, P.B., Gage, J.D., 2003. The cold-water coral *Lophelia pertusa* (Scleractinia) and enigmatic seabed mounds along the north-east Atlantic margin: are they related? Mar. Pollut. Bull. 46, 7–20.

Roberts, J.M., Wheeler, A.J., Freiwald, A., 2006. Reefs of the deep: the biology and geology of cold-water coral ecosystems. Science 312, 543–547.

Roberts, J.M., Wheeler, A.J., Freiwald, A., Cairns, S.D., 2009. Cold-water Corals. The Biology and Geology of Deep-sea Coral Habitats. Cambridge University Press, Cambridge, UK.

Romero, O.E., Kim, J.-H., Donner, B., 2008. Submillennial-to-millennial variability of diatom production off Mauritania, NW Africa, during the last glacial cycle. Paleoceanography 23, PA3218.

Roudier, P., Ducharne, A., Feyen, L., 2014. Climate change impacts on runoff in West Africa: a review. Hydrol. Earth Syst. Sci. 18, 2789–2801.

Sanz, J.L., Maestro, A., Agudo, L.M., 2017. The Mauritanian margin. Bathymetric and geomorphological characteristics. In: Ramos, A., Ramil, F., Sanz, J.L. (Eds.), Deep-sea Ecosystems off Mauritania: Research of Marine Biodiversity and Habitats in the Northwest African Margin. Springer Netherlands, Dordrecht, pp. 53–117.

Stramma, L., Hüttl, S., Schafstall, J., 2005. Water masses and currents in the upper tropical northeast Atlantic off northwest Africa. J. Geophys. Res.: Oceans 110, C12. https://doi.org/10.1029/2005JC002939.

Stramma, L., Johnson, G.C., Sprintall, J., Mohrholz, V., 2008. Expanding oxygen-minimum zones in the tropical oceans. Science 320, 655.

Stramma, L., Schott, F., 1999. The mean flow field of the tropical Atlantic Ocean. Deep-Sea Res. Part II 46, 279–303.

Taviani, M., Angeletti, L., Beuck, L., Campiani, E., Canese, S., Foglini, F., Freiwald, A., Montagna, P., Trincardi, F., 2016. Reprint of 'On and off the beaten track: megafaunal sessile life and Adriatic cascading processes'. Mar. Geol. 375, 146–160.

Thierens, M., Browning, E., Pirlet, H., Loutre, M.F., Dorschel, B., Huvenne, V.A.I., Titschack, J., Colin, C., Foubert, A., Wheeler, A.J., 2013. Cold-water coral carbonate mounds as unique palaeo-archives: the Plio-Pleistocene Challenger Mound record (NE Atlantic). Quat. Sci. Rev. 73, 14–30.

Thresher, R.E., Tibrook, B., Fallon, S., Wilson, N.C., Adkins, J.F., 2011. Effects of chronic low carbonate saturation levels on the distribution, growth and skeletal chemistry of deep-sea corals and other seamount megabenthos. Mar. Ecol. Prog. Ser. 442, 87–99.

Titschack, J., Baum, D., De Pol Holz, R., López Correa, M., Forster, N., Flögel, S., Hebbeln, D., Freiwald, A., 2015. Aggradation and carbonate accumulation of Holocene Norwegian cold-water coral reefs. Sedimentology 62, 1873–1898.

Titschack, J., Fink, H.G., Baum, D., Wienberg, C., Hebbeln, D., Freiwald, A., 2016. Mediterranean cold-water corals – an important regional carbonate factory? Depositional Record 2, 74–96.

Titschack, J., Thierens, M., Dorschel, B., Schulbert, C., Freiwald, A., Kano, A., Takashima, C., Kawagoe, N., Li, X., 2009. Carbonate budget of a cold-water coral mound (Challenger Mound, IODP Exp. 307). Mar. Geol. 259, 36–46.

Tomczak, M., 1984. Ausbreitung und Vermischung der Zentralwassermassen in den Tropengebieten der Ozeane. 1: atlantischer Ozean. Oceanol. Acta 7, 145–158.

Turley, C.M., Roberts, J.M., Guinotte, J.M., 2007. Corals in deep-water: will the unseen hand of ocean acidification destroy cold-water ecosystems? Coral Reefs 26, 445–448.

Urlaub, M., Talling, P.J., Zervos, A., Masson, D., 2015. What causes large submarine landslides on low gradient (<2°) continental slopes with slow (~0.15 m/kyr) sediment accumulation? J. Geophys. Res.: Solid Earth 120, 6722–6739.

van der Land, C., Eisele, M., Mienis, F., de Haas, H., Hebbeln, D., Reijmer, J.J.G., van Weering, T.C.E., 2014. Carbonate mound development in contrasting settings on the Irish margin. Deep Sea Res. Part II 99, 297–306.

Vandorpe, T., Wienberg, C., Hebbeln, D., Van den Berghe, M., Gaide, S., Wintersteller, P., Van Rooij, D., 2017. Multiple generations of buried cold-water coral mounds since the early-middle pleistocene transition in the atlantic moroccan coral province, southern Gulf of cádiz. Palaeogeogr. Palaeoclimatol. Palaeoecol. 485, 293–304.

Victorero, L., Blamart, D., Pons-Branchu, E., Mavrogordato, M.N., Huvenne, V.A.I., 2016. Reconstrcution of the formation history of the Darwin Mounds, N Rockall Trough: how the dynamics of a sandy contourite affected cold-water coral growth. Mar. Geol. 378, 186–195.

Wefing, A.-M., Arps, J., Blaser, P., Wienberg, C., Hebbeln, D., Frank, N., 2017. High precision U-series dating of scleractinian cold-water corals using an automated chromatographic U and Th extraction. Chem. Geol. 475, 140–148.

Westphal, H., Beuck, L., Braun, S., Freiwald, A., Hanebuth, T., Hetzinger, S., Klicpera, A., Kudrass, H., Lantzsch, H., Lundälv, T., Vicens, G.M., Preto, N., von Reumont, J., Schilling, S., Taviani, M., Wienberg, C., 2012. Phaeton - Paleoceanographic and Paleo-climatic Record on the Mauritanian Shelf – Cruise No. MSM16/3-oct 13 – Nov 20, 2010-Bremerhaven (Germany) – Mindelo (Cap Verde). MARIA S. MERIAN-Berichte, p. 54. https://doi.org/10.2312/cr_msm16_3. MSM16/3, 57 pp., DFG-Senatskommission für Ozeanographie.

Westphal, H., Freiwald, A., Hanebuth, T., Eisele, M., Gürs, K., Heindel, K., Michel, J., Reumont, J.V., 2007. Report and Preliminary Results of Poseidon Cruise 346-MACUMA: Integrating Carbonates, Siliciclastics and Deep-water Reefs for Understanding a Complex Environment, Las Palmas (Spain), 28.12.2006-15.1.2007. Reports of the Dept. of Geosciences. University of Bremen, Bremen, p. 49.

Wheeler, A.J., Beyer, A., Freiwald, A., de Haas, H., Huvenne, V.A.I., Kozachenko, M., Olu-Le Roy, K., Opderbecke, J., 2007. Morphology and environment of cold-water coral carbonate mounds on the NW European margin. Int. J. Earth Sci. 96, 37–56.

White, M., Mohn, C., de Stigter, H., Mottram, G., 2005. Deep-water coral development as a function of hydrodynamics and surface productivity around the submarine banks of the Rockall Trough, NE Atlantic. In: Freiwald, A., Roberts, J.M. (Eds.), Cold-water Corals and Ecosystems. Springer, Heidelberg, pp. 503–514.

Wien, K., Kölling, M., Schulz, H.D., 2007. Age models for the Cape Blanc debris flow and the Mauritania slide complex in the Atlantic Ocean off NW africa. Quat. Sci. Rev. 26, 2558–2573.

Wienberg, C., Frank, N., Mertens, K.N., Stuut, J.-B., Marchant, M., Fietzke, J., Mienis, F., Hebbeln, D., 2010. Glacial cold-water coral growth in the Gulf of Cádiz: implications of increased palaeo-productivity. Earth Planet Sci. Lett. 298, 405–416.

Wienberg, C., Hebbeln, D., Fink, H.G., Mienis, F., Dorschel, B., Vertino, A., López Correa, M., Freiwald, A., 2009. Scleractinian cold-water corals in the Gulf of Cadiz-First clues about their spatial and temporal distribution. Deep-Sea Res. Part I 56, 1873–1893.

Wienberg, C., Titschack, J., 2017. Framework-forming scleractinian cold-water corals through space and time: a late Quaternary North Atlantic perspective. In: Rossi, S., Bramanti, L., Gori, A., Orejas Saco del Valle, C. (Eds.), Marine Animal Forests: the Ecology of Benthic Biodiversity Hotspots. Springer, Cham, pp. 699–732.

Wintersteller, P., Titschack, J., Gaide, S., Hanebuth, T.J.J., Freiwald, A., Westphal, H., 2017. Gridded EM1002 Multibeam-echosounder Bathymetry of Cruise MSM16-3. PANGAEA (unpublished data set). https://doi.pangaea.de/10.1594/PANGAEA.883754.

Zenk, W., Klein, B., Schroder, M., 1991. Cape Verde frontal zone. Deep Sea Res. Part A 38 (Suppl. 1), S505–S530.